



Research article

Late Miocene stratigraphy, palaeoclimate and evolution of the Sandanski Basin (Bulgaria) and the chronology of the Pikermian faunal changes

Madelaine Böhme^{a,b,*}, Christiaan G.C. Van Baak^{c,d}, Jérôme Prieto^e, Michael Winklhofer^f, Nikolai Spassov^g

^a Terrestrial Palaeoclimatology, Department of Geosciences, Eberhard-Karls-University Tübingen, Sigwartstrasse 10, 72076 Tübingen, Germany

^b Palaeontology, Senckenberg Centre for Human Evolution and Palaeoenvironment, Sigwartstrasse 10, 72076 Tübingen, Germany

^c Palaeomagnetic Laboratory 'Fort Hoofdijk', Faculty of Geosciences, Utrecht University, Budapestlaan 17, 3584 CD Utrecht, the Netherlands

^d CASP, West Building, Madingley Rise, Madingley Road, Cambridge CB3 0UD, United Kingdom

^e Palaeontology, Department of Earth and Environmental Sciences, Ludwig-Maximilians-University, Richard-Wagner-Strasse 5, 80333 Munich, Germany

^f School of Mathematics and Science, Institute of Biology and Environmental Science, University of Oldenburg, Germany

^g National Museum of Natural History, Bulgarian Academy of Sciences, Tzar Osvoboditel 1, 1000 Sofia, Bulgaria

ARTICLE INFO

Keywords:

Late Miocene
Magnetostatigraphy
Pikermian mammals
Faunal change
Sahara dust

ABSTRACT

We study the sedimentology, palaeontology and palaeomagnetism of the 500 m thick sedimentary sequence in the Gorna Sushitsa gorge in the Sandanski Basin (southwest Bulgaria), which is exceptionally rich in fossil mammals of Pikermian type. Magnetostatigraphy indicates that this section was deposited within 2 myrs, between 8.5 Ma and 6.5 Ma (late Tortonian to early Messinian). Our investigations reveal that the Sandanski Basin infill represents two stacking synrift phases (Delcevo and Kalimantsi formations), with an intervening tectonic quiescence package (Sandanski Formation). Kalimantsi Formation deposition ends with the cessation of slip on basin-bounding faults at 6.9 Ma, probably caused by a switch from regional E-W to N-S extension between 7 and 6.5 Ma. High slip rates compared to hanging wall sedimentation rates induced the development of mega-breccia dominated substantial fault scarps during the younger synrift phase (8.2 to 6.9 Ma). Tectonic changes are superimposed by several climatic changes. Moderately humid conditions prevail from 8.5–8.2 Ma, followed by relatively dry period from 8.2 to 7.8 Ma. A second humid interval from 7.74–7.56 Ma, which may be responsible for the Maeotian transgression in the Eastern Paratethys lake, is followed by a significant trend in local and supra-regional aridization, indicated by the onset of orbital driven aeolian dust deposition at 7.42 Ma. Our new data expand the Northern Mediterranean Sahara-born dust record at the Tortonian-Messinian transition to at least 600 kyrs (7.42 to 6.85–6.8 Ma). Coeval with the onset of dust deposition we observed evolutionary changes in the large mammal record, leading to the classical Pikermian association dated to between 7.42 and 7.27 Ma. We interpret faunal changes at the Tortonian-Messinian transition in the Eastern Mediterranean as driven by global cooling and mid-latitude desertification.

1. Introduction

The Sandanski Basin in SW Bulgaria is a half-graben structure situated in the northwestern part of the extensional South Rhodope core complex (SRCC) of the southern Balkan Peninsula (Burchfiel et al., 2003; Zagorchev, 2007). The SRCC is linked to the Cenozoic back-arc extension in the Aegean (Zagorchev, 1992; Dinter, 1998; Burchfiel et al., 2000; Kounov et al., 2015), and its extension is accommodated by the Paleogene Kerdillion and Mesta detachments and the Miocene Strymon-Gorno Spanchevo detachment (Kounov et al., 2015; Stübner

et al., 2016). The Sandanski basin develops in the hanging walls of the Strymon-Gorno Spanchevo detachment and the West Pirin Fault (Fig. 1; Zagorchev, 1992; Westaway, 2006).

First fossil mammals from the Sandanski Basin have been found near Kalimantsi and Kromidovo in the southern part of the Basin. Announced by Drenovski (1932) and described by Bakalov (1933, 1934a, 1934b, 1939, 1953), both localities represent the first 'Pikermian-type' assemblages known from Bulgaria. With the intensification of fieldwork the number of localities steadily increased to six (Bakalov and Nikolov, 1962), 15 (Nikolov, 1985) and 24 (Tzankov et al., 2005), presenting the

* Corresponding author at: Terrestrial Palaeoclimatology, Department of Geosciences, Eberhard-Karls-University Tübingen, Sigwartstrasse 10, 72076 Tübingen, Germany.

E-mail address: m.boehme@ifg.uni-tuebingen.de (M. Böhme).

<https://doi.org/10.1016/j.gloplacha.2018.07.019>

Received 11 May 2018; Received in revised form 25 July 2018; Accepted 31 July 2018

Available online 01 August 2018

0921-8181/ © 2018 Elsevier B.V. All rights reserved.

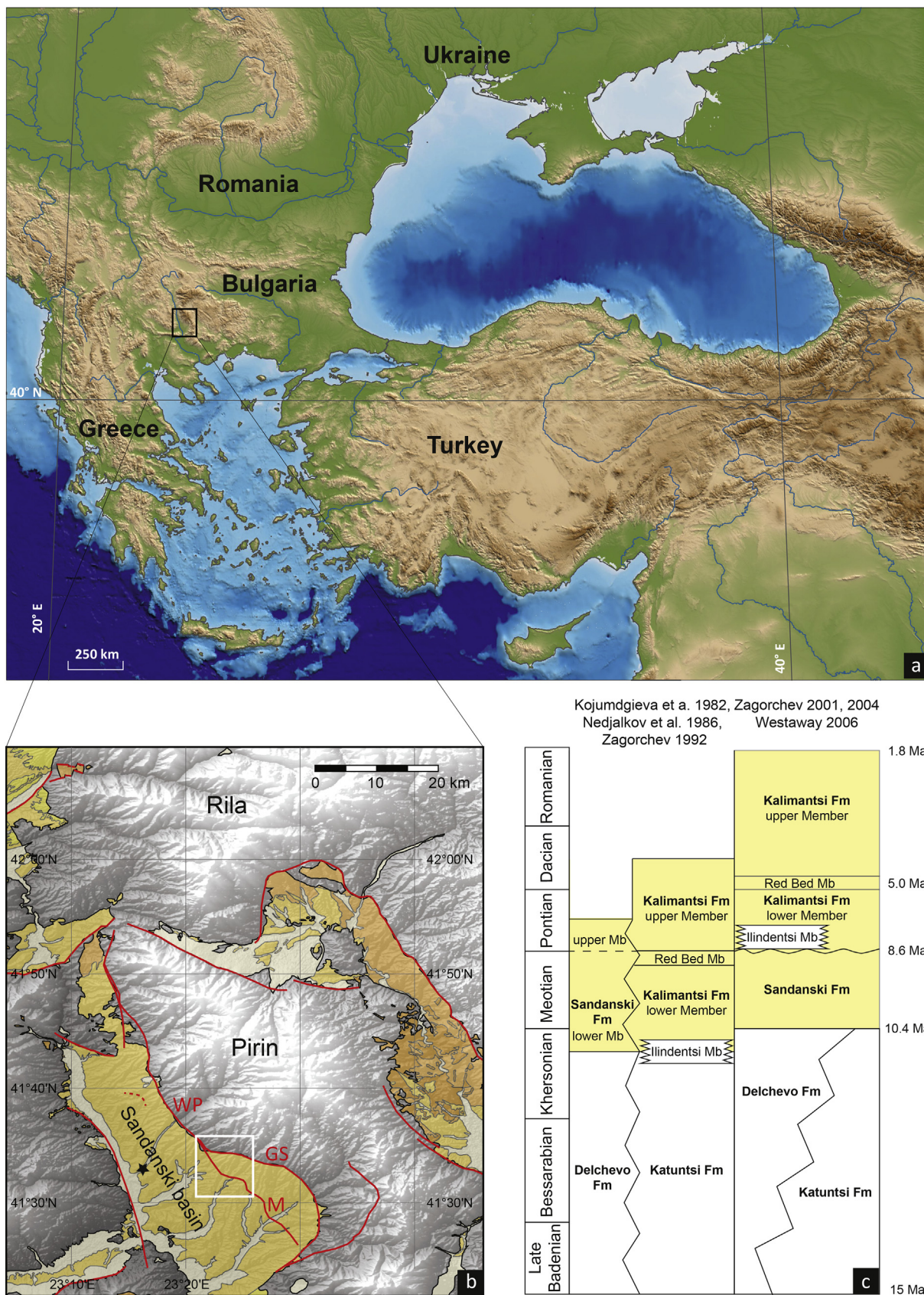


Fig. 1. a) Topographic and bathymetric overview map of the Aegean and Black Sea region. b) topographic map of southwest Bulgaria highlighting the sedimentary fill of Sandanski and surrounding basins (according to Zagorchev and Dinkova, 1990, modified after Stübner et al., 2016; Paleogene, orange; Neogene, yellow; Quaternary, buff). The white box represent the work area and the black star the city of Sandanski. Abbreviations are M, Melnik fault; GS, Gorno Spanchevo fault; WP, West Pirin fault. The dashed red line represent the distribution of the „Ilindentsi Member“ (see text for explanation). c) Lithostratigraphic subdivision and chronostratigraphic correlation of Neogene deposits of the Sandanski Basin according to different authors (yellow highlights the stratigraphy covered in this study). (For interpretation of the references to colour in this figure legend, the reader is referred to the web version of this article.)

Sandanski Basin as one of the most appropriate places to study late Miocene mammalian evolution in the circum-Mediterranean.

According to Kostopolous (2009) large mammal assemblages from the Balkans remain relatively distinct from their Anatolian counterparts of the so-called sub-Paratethyan bioprovince during most of the late Miocene. However, during the short period of the middle Turolian the Balkan became part of the sub-Paratethyan bioprovince, referred by him to as the Pikermian Large Mammal Event. Kostopolous (2009) relates this renewal of the large mammal fauna and the subsequent decline in faunal similarity to overall climatic changes and physio-geographic factors, namely the opening and intermission of the Aegean Sea. Spassov et al. (2012) and Böhme et al. (2017) have shown that the Pikermian faunas from the Balkan area are punctuated by an additional turnover event at the Tortonian-Messinian boundary, separating the ‘classical Pikermian fauna’ (7.33–7.27 Ma) from the ‘post-Pikermian fauna’ (7.26–7.15 Ma). Böhme et al. (2017) relate this turnover event to an interval of global cooling (Tzanova et al., 2015) and the initiation of intensive North African and Arabian desertification, leading to the partial replacement of Pikermian taxa by West Asian immigrants, among them the first potential hominins (Fuss et al., 2017).

All previous fossil mammal investigations in the Balkans were conducted on short stratigraphic sections or without stratigraphic or geologic control, significantly lowering the potential biostratigraphic value of recovered fossil large mammals. Our present investigation of the Sandanski Basin is significant, because the thickness of the basin sediments has been estimated to > 1600 m (Kojumdgieva et al., 1982; Zagorchev, 1992). These exceptionally thick deposits provide excellent outcrop conditions in deeply eroded gullies. However, the exact chronology of these sediments and their containing fauna remains elusive, varying according different authors between 15 and 0.5 Ma (Fig. 1). Since better age control is crucial for understanding the timing of crustal extension and basin formation, as well as for constraining the evolution of fauna, landscape and climate, we study the geology, sedimentology and magnetostratigraphy of the Gorna Sushitsa gorge (Fig. 2). With 500 m stratigraphic thickness, the Gorna Sushitsa gorge (near the village of Gorna Sushitsa) represents one of the longest, most continuously exposed outcrop records of the Sandanski Basin and the Balkan Peninsula in general. This type of long continental record has the potential to provide important age constraints for palaeoenvironmental and faunal evolution. Here, we aim to clarify the stratigraphy of the younger basin infill and to understand the role of tectonics and climate on depositional environments. We provide a robust, independent age model for stratigraphic units and the fossil mammal faunas and discuss our results in the wider regional context within the Mediterranean and Paratethyan realm. With our new data, we further evaluate the chronology and possible driving mechanisms of the Pikermian Event and its possible significance for early hominin evolution.

2. Geological background

For the northern SRCC, Stübner et al. (2016) suggest three stages of Cenozoic NE-SW extension. 1) Eocene/Oligocene (> 28 Ma) extension accommodated by the Mesta detachment with *syn*-extensional intrusion of granitic plutons and formation of the Palaeogene Mesta half-graben; 2) early to middle Miocene (18–15 Ma) rapid extension along the Gorno Spanchevo-Strymon low-angle detachment without *syn*-extensional basin formation, and 3) activation of the steeply dipping West Pirin and Melnik faults during the Late Miocene (10–7 Ma), leading to the formation of the Sandanski half-graben and to significant uplift and erosion of the metamorphic footwall (Pirin mountains). Erosional exhumation during this stage is calculated to be ≥ 2.5 km in the northern and central Pirin.

The basic lithostratigraphy of the Sandanski half-graben was introduced by Kojumdgieva et al. (1982) and supplemented by Nedialkov et al. (1986). These authors subdivide the generally E to NE dipping Neogene sediments into four formations, including six members

(Fig. 1c). The basal Delcevo Formation represents weakly cemented conglomerates, sandstones and siltstones of dominantly red colour, with grey and green interbeds (Kojumdgieva et al., 1982). The Katuntsi Formation consists of red conglomerates and breccia-conglomerates, interpreted as a proluvial facies proximal to the alluvial Delcevo Formation (Nedialkov et al., 1986). The overlying Sandanski Formation is defined as an irregular alternation of partly carbonate-cemented, relatively well sorted medium- to fine-grained conglomerates, sandstones, siltstones and rarely clay and coal, where green and grey-green colours dominate the fine fraction and whitish to yellowish colours the coarse fractions. The Kalimantsi Formation consists of poorly sorted, massive conglomerates and breccia-conglomerates, interpreted as a proluvial facies proximal to the alluvial Sandanski Formation (Kojumdgieva et al., 1982). According to Kojumdgieva et al. (1982) the Sandanski and Kalimantsi formations include two fining-upward cycles (introduced as ‘lower member’ and ‘upper member’, respectively) and both members of the Kalimantsi Formation are separated by a ‘red bed unit’ (10–15 m, up to 200 m) of reddish unsorted silty sandstones and siltstones with fine-pebble conglomerates. Furthermore, Nedialkov et al. (1986) introduce the Ilindentsi Member at the base of the Kalimantsi Formation. This member (with inferred thickness of 50–70 m) represents a well-cemented monomictic marble-breccia (coarse and huge blocks up to tens of meters in size), which grade laterally into oligomictic breccias (with marble, amphibolite, gneiss). This member is distributed only in the northern part of the basin (near the villages Ilindentsi and Ploski) along a 5 km long strip (red dashed line in Fig. 1b). The marble derives from the Dobrostan Formation from the adjacent foothills of the West Pirin Fault (Zagorchev, 2007). In contrast to the lithostratigraphic subdivision of Kojumdgieva et al. (1982) and Nedialkov et al. (1986), later authors (e.g. Zagorchev and Dinkova, 1990; Zagorchev, 2001) suppose a superposition of the Sandanski Formation by the Kalimantsi Formation, instead of their lateral equivalence.

There is no active slip on the West Pirin and Gorno Spanchevo Fault (Zagorchev, 1992; Westaway, 2006). After Zagorchev (1992), both faults are sealed in places with westward dipping Early Pleistocene sediments. Digital topographic analysis of river channel profiles of Stübner et al. (2016) revealed no Pleistocene slip on the West Pirin Fault, but possible Quaternary activation of the Melnik Fault.

3. Material and methods

3.1. Study area

For a study area we selected the Gorna Sushitsa gorge, 9 km East of Sandanski and 3 km North of Melnik. This gorge provides accessible outcrop conditions of the upper 500 m of basin infill, and it includes the Melnik Fault, the most prominent tectonic feature of the basin. Furthermore, outcropping sediments are rich in fossil vertebrates. We studied the sedimentary succession exposed in six sub-sections (A–F). Two sub-sections (A and E) are in the hanging wall of the Melnik Fault and four sub-sections (B–D, F) are in its footwall (Fig. 2).

3.2. Paleomagnetism

Over the course of multiple fieldworks, a total of 141 levels were sampled in the field using a battery-powered drill, taking multiple oriented, standard palaeomagnetic samples per investigated horizon. This gives an average sampling resolution of around one sample every 3–3.5 m. Samples were taken from the finest grained sediments available at regularly spaced intervals.

All palaeomagnetic analyses were conducted at the Palaeomagnetic Laboratory “Fort Hoofdijk” at Utrecht University, The Netherlands. Magnetic susceptibility measurements were performed on an AGICO MultiFunction Kappabridge (MFK) 1-FA at room temperature. To determine the thermal behavior of the magnetic carriers, thermomagnetic measurements were performed on a representative number of samples

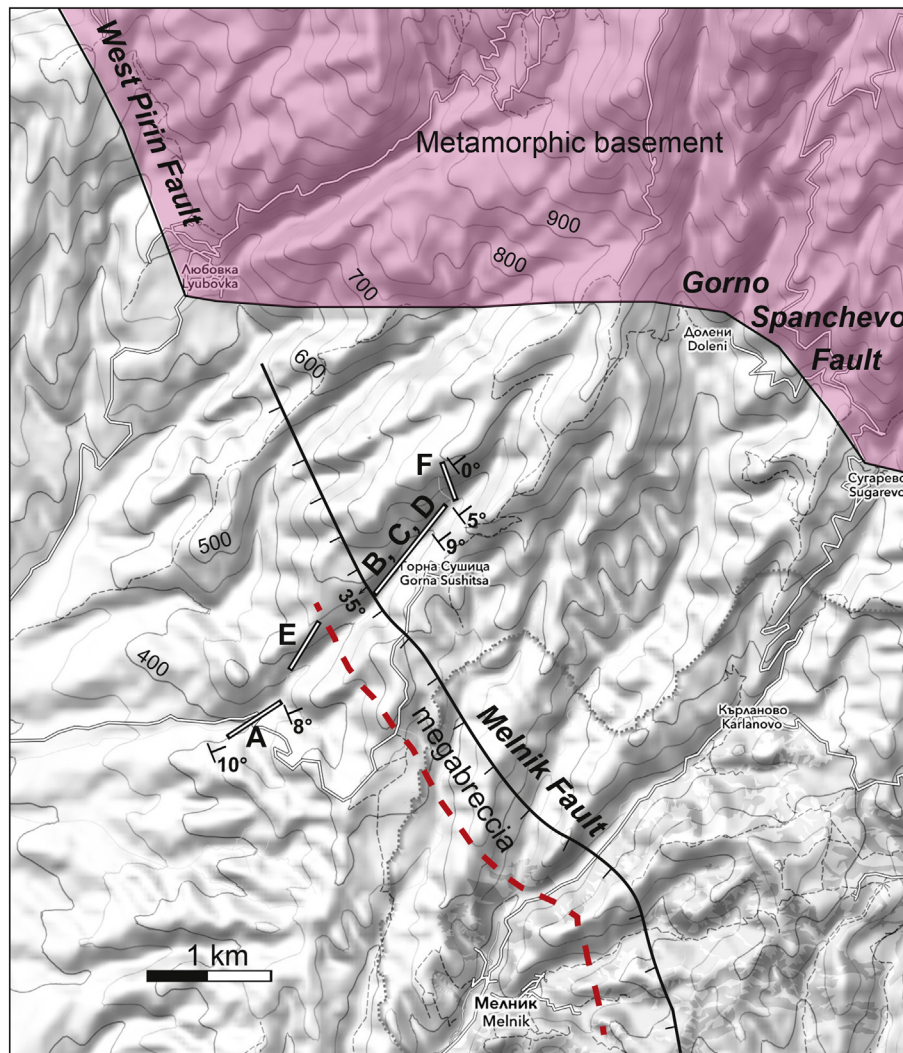


Fig. 2. Topographic map of the studied region showing the sampled sub-sections A to F and the distribution of the massive syntectonic megabreccia (red dashed line). (For interpretation of the references to colour in this figure legend, the reader is referred to the web version of this article.)

in air on a modified horizontal translation type Curie balance (noise level $5 \times 10^{-9} \text{Am}^2$) (Mullender et al., 1993). Following this, a total of 113 specimens were stepwise thermally demagnetized in a magnetically shielded, laboratory-built, furnace, using temperature increments of 20–60°C with successively smaller steps at higher temperatures. The maximum temperature reached for demagnetization was 640°C, although the majority of samples were already completely demagnetized at 580°C. After each thermal treatment, the remanent magnetization was measured on a horizontal 2G Enterprises DC SQUID cryogenic magnetometer (noise level $3 \times 10^{-12} \text{Am}^2$). All directional interpretations and statistical analysis of the palaeomagnetic results were performed using the Paleomagnetism.org interpretation portal (Koymans et al., 2016).

In an earlier stage of the laboratory process, separate samples were demagnetized using alternating field demagnetization. This was performed on an in-house built robotized sample handler controller attached to a horizontal 2G Enterprises DC SQUID cryogenic magnetometer (Mullender et al., 2016). Results from these experiments are not presented, as they did not provide the same analytical quality as the thermal experiments.

3.3. Grain-size analysis

To determine the contribution of aeolian dust to palaeosols from

grain-size spectra, we collected 34 sediment samples from the Orange Interval (sub-section C) at a stratigraphic resolution of 2 to 3 m. Particle size distributions were determined with a Laser Particle Sizer (Mastersizer 2000, Malvern Instruments, University of Tübingen) using Sodiumpyrophosphate ($\text{Na}_4\text{P}_2\text{O}_7 \cdot 10 \text{H}_2\text{O}$) as a dispersant. Pre-treatment of samples (including decalcification) was performed according to Konert and Vandenberghe, 1997. The 34 grain-size spectra were subject to end-member analysis (Weltje and Prins, 2007; Dietze and Dietze, 2013) to identify sedimentologically distinct components (end members) that explain most of the variance in all measured grain-size spectra. As described in more detail in Böhme et al. (2017), we use EMMAgeo (Dietze and Dietze, 2013) to obtain a first model of robust end-member factor loadings (grain-size distribution). Endmembers found that way are usually not characterized by a unimodal grain-size spectrum, but have subordinate modes overlapping with the main mode of another end member. Therefore, to obtain distinct components, we select the main modes, approximated by a log-normal distribution (Supplementary Data 1).

3.4. Fossil fauna

The small mammals (GB levels in sub-section A; Fig. 3), plant and ichnological fossils described in this publication are stored in the Palaeontological Collection of Tübingen University (acronym GPIT). Large

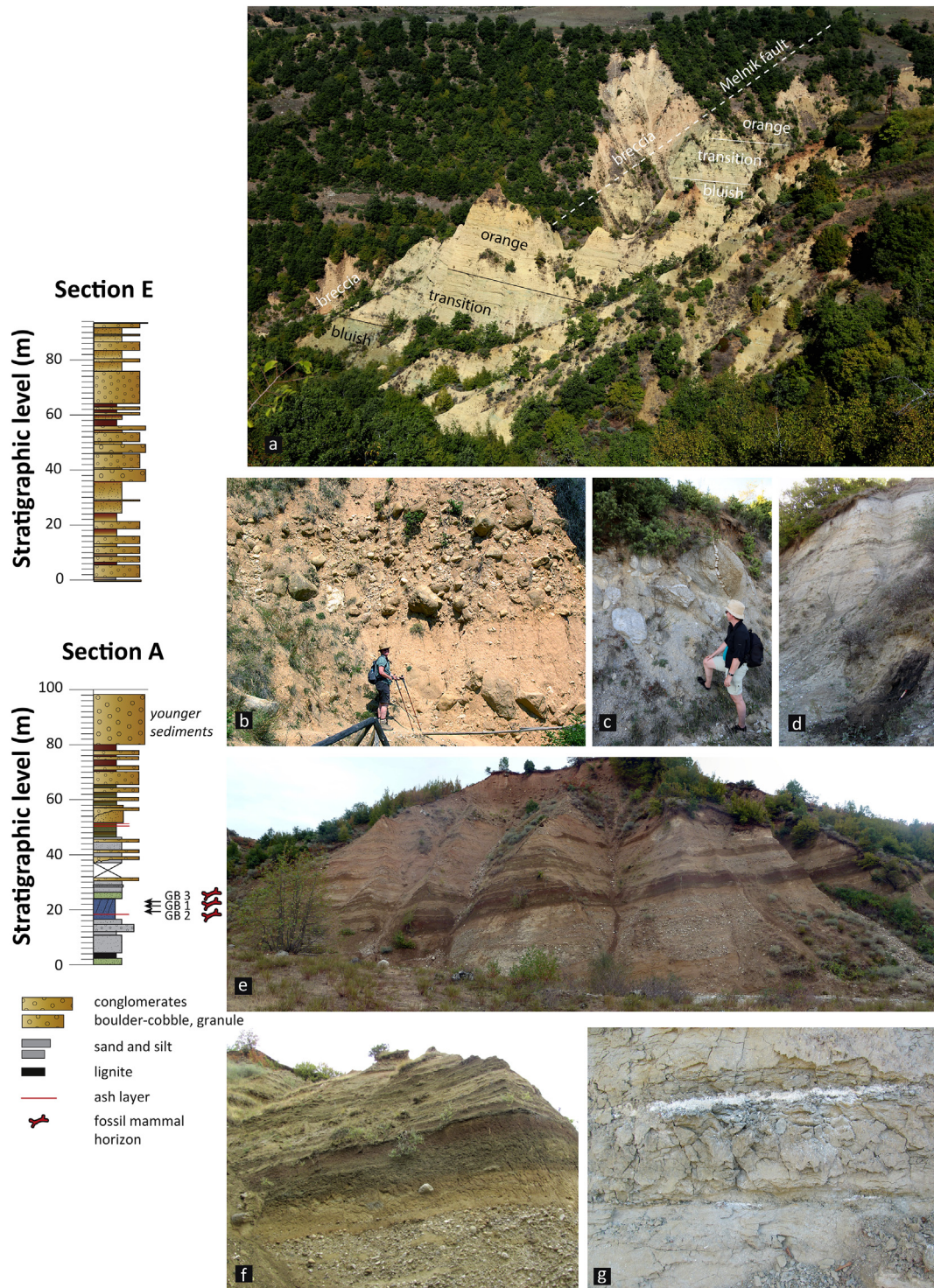
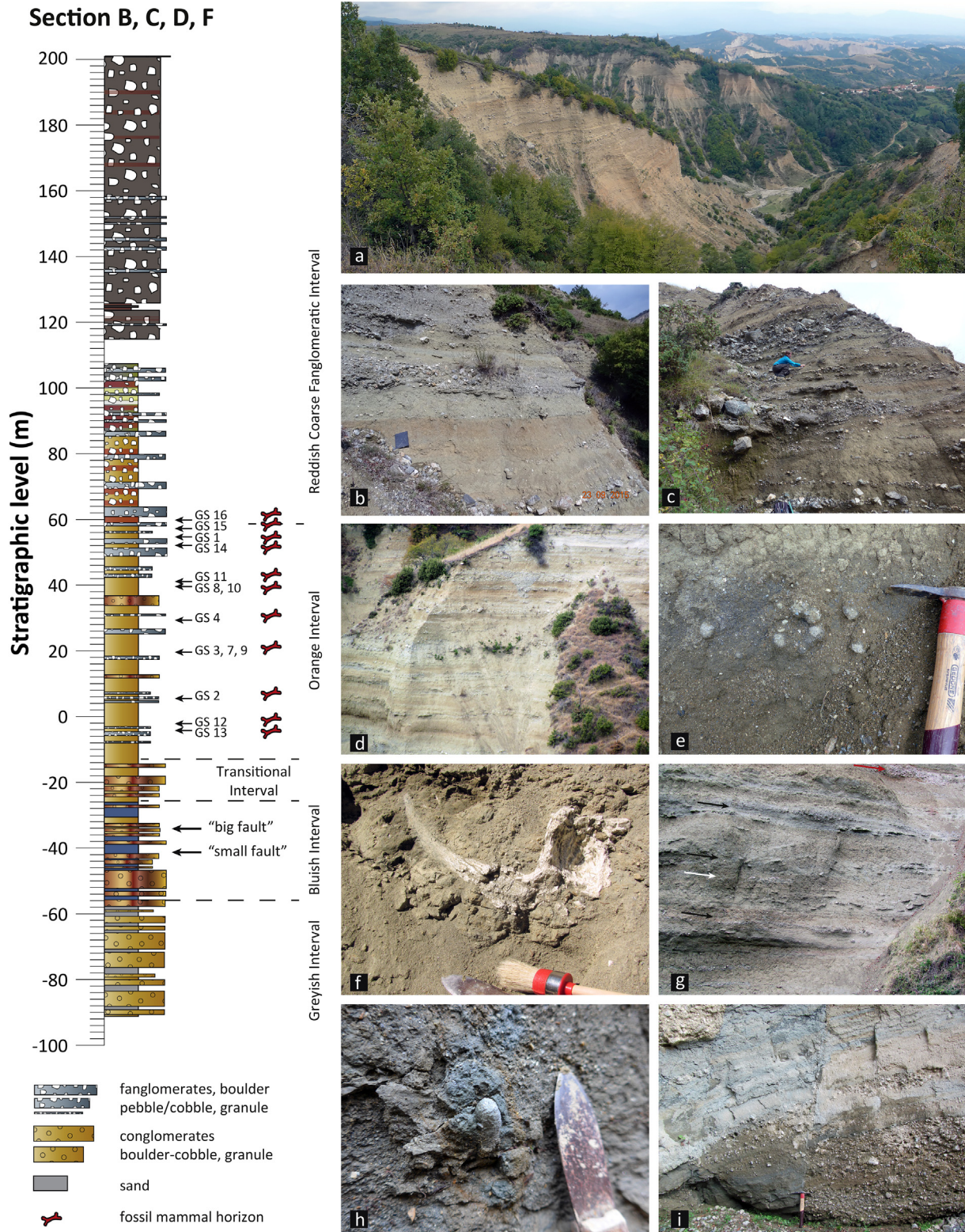


Fig. 3. a) View into the Gorna Sushitsa gorge towards NW showing the NNW-SSE trending Melnik fault (dip 35°) and the footwall sedimentary succession (dip 10–8°) of Bluish-, Transition-, and Orange Intervals. b)-g) Images for Gorna Sushitsa sections A and E. b) Lobe of syntectonic megabreccia in the footwall of the Melnik fault (2.5 km ENE of Melnik). c) Massive megabreccia in the hanging wall of the Melnik fault (850 m SSW of Gorna Sushitsa). d) Lignite horizon from the base of section A (hammer for scale). e) View of the upper part of section A with well-developed yellow-green-to-red palaeosols and cobble size conglomerates. The uppermost 11 m represent an erosional package of block-sized breccias. f) Detail view on yellow-green-to-red palaeosol (stratigraphic level 56 to 65) with floating cobble in the yellow C-horizon. g) Ash layer (2 cm thick) from section A at stratigraphic level 18.3. (For interpretation of the references to colour in this figure legend, the reader is referred to the web version of this article.)



mammals from GS levels (in sub-section C; Fig. 4), not described here, are deposited in the National Museum of Natural History (Sofia).

4. Results

4.1. Section description

The most characteristic geologic feature of the Gorna Sushitsa gorge is the appearance of a mega-breccia (Fig. 3a–c), which outcrops as a massive unit in a 500 m wide NNW-SSE trending strip. It is observable in over 50 m high cliffs south-eastwards of Melnik (Fig. 2). This unit appears as a chaotic assemblage of clast-supported, highly weathered angular and rounded granite boulders and blocks (Fig. 3c), reaching up to 2.5 m (a single case of 4 m) in size. The matrix is composed of brownish fine sand. We identify the mega-breccia as the hanging-wall sedimentation along a moderately dipping (35°) fault (Fig. 3a). Similar geologic structures north and northeast of Melnik associate this breccia with the Melnik Fault (Vrablianski, 1969), which we traced in the field over 7 km. As already observed by Kojumdjieva et al. (1982, pp. 74) individual lobes of the mega-breccia can be observed up to 2 km south of the fault, but also on its footwall, where they interfinger with bedded deposits (Fig. 3b).

The 98 m thick section A shows in its lower 30 m predominantly silty and fine-sandy lithologies of greenish, bluish, to greyish colours, including a 2 m thick lignitic horizon near its base (Fig. 3d). The top 30 cm of this horizon contain, in a silt-clay matrix, well-preserved plant remains (Cyperaceae, Nymphaeaceae) indicating shallow-lacustrine and marsh conditions. Two white ash layers, 0.5 and 2 cm thick are found in fine laminated bluish silts between 18 and 18.5 m (Fig. 3g). All fine clastic sediments have a varying proportion of clay and fine sand and show regularly spaced (~0.5 m) thin layers of coarse sand or fine gravel. We found three vertebrate fossil layers (GB 1–3) directly above the ash layers. The middle part of section A (30–80 m) is characterized by well-rounded coarse gravel horizons of granitic composition showing erosional bases, alternating with up to 2 m thick fine grained deposits (Fig. 3e). These deposits are usually tripartite by pedogenic overprint (Fig. 3f). The lower 0.8 m are yellowish sands containing fine-gravels, followed by 0.7 m greenish-yellowish mottled fine sand and 0.5 m of reddish clayey silt. Steeply dipping sparitic calcite veins crosscut both upper soil horizons. Three thin (0.5 to 2 cm) white ash layers are found between stratigraphic meter 50 and 52. The upper part of section A shows a channelized erosional unconformity. The loosely consolidated channel fill represents chaotic conglomerates and breccias and consists of two fining upward cycles. The clasts of the lower cycle (11 m thick) range from boulder to coarse cobble size (0.5 to 0.2 m), whereas the upper cycle (> 7 m thick) starts with angular blocks of up to 1.5 m size. Sediments of section A dip 8° to 10° towards northeast (Fig. 3e).

Section E is 94 m thick and characterized by well-rounded component or matrix supported conglomerates in the size of coarse cobbles (0.2–0.25 m). Between stratigraphic meters 36–40, 46–48, and 65–76, boulder-sized (up to 1.2 m) conglomerates and breccias appear. Conglomerate packages alternate with silty fine sands of yellowish to reddish colours, with most intense red chroma between stratigraphic meters 53 and 64. Finer sediments commonly contain granule to pebble-size interlayers, which are frequently carbonate cemented.

In the footwall of the Melnik Fault, we measured a 292 m thick composite section (sub-sections B–D, F; base of sub-section C is stratigraphic level 0 m). Based on the predominant colour of fine-grained sediments we subdivided the section into five intervals (Fig. 4): Greyish Interval (between stratigraphic meters –92 and –58), Bluish Interval (between stratigraphic meters –58 and –26), Transitional Interval (between stratigraphic meters –26 and –13), Orange Interval (between stratigraphic meters –13 and 58), and Reddish Coarse Fanglomeratic Interval (between stratigraphic meters 58 and 200).

The *Greyish Interval* is characterized by grey to greyish-brownish

mottled fine sands in alternation with poorly to unsorted debris of sub-angular to rounded cobbles to boulders (0.2 to 0.3 m). Occasional blocks of 1.5 m diameter occur (stratigraphic meter –68).

The *Bluish Interval* is characterized by blue-grey to grey, rarely mottled fine and middle sands, which are intercalated between unsorted debris of sub-angular to rounded cobbles to boulders (lower part up to stratigraphic meter –47) and well-rounded cobble-size conglomerates (upper part). Several thin (2 cm) brown clay horizons appear at stratigraphic meter –32, below which we found the insect ichnogenus *Celliforma*. We also observed two steeply (80°) NE-dipping normal faults, with maximum offset of 4 m ('big fault', Fig. 4i).

The *Transitional Interval* is characterized by blue grey-reddish/orange mottled medium to fine sand. The coarse fraction consists of cobble-size rounded conglomerates or/and boulder-size (0.4 m) sub-angular and poorly sorted breccia-conglomerates with an erosional base.

The *Orange Interval* typifies yellowish-reddish (orange; rarely greenish-grey) fine sand (litharenite) and the near lack of conglomerates (except at stratigraphic meters 12 and 34 to 37). Instead, very angular fanglomerates of granitic and amphibolitic petrology (no carbonates) appear. In its lower part (stratigraphic meters –13 to 48) fanglomerates are of cobble size and appear in widely spaced thin beds of 0.3 to 1.5 m thickness (Fig. 4g). In the upper part of the orange interval (stratigraphic meters 48 to 58) fanglomerates are of boulder size (up to 0.4 m) with thicker beds. Single cobble to boulder-sized floating stones are common in the litharenites, as well as the ichnofossil *Celliforma* (Fig. 4f). Vertical cylindrical burrows (cf. *Planolites*) are rarely observed. Pedogenic carbonate content is present in places, but generally low. Instead, 2 cm size nodular carbonate cemented litharenites, interpreted as groundwater calcretes (Fig. 4e), are common in some horizons (highest at stratigraphic meter 55). However, the most conspicuous feature of the orange interval are regularly occurring mammal bone accumulations (Fig. 4f). We identify 16 localities (GS 1–16), belonging to 11 bone layers (Fig. 4). The dip of the sediments of the Orange Interval is 9° towards NE.

The *Reddish Coarse Fanglomeratic Interval* is further characterized by an increase in fanglomerate particle size (boulders, blocks up to 2.5 m size; Fig. 4c) and density (above stratigraphic meter 110 individual horizons are hardly distinguishable; Fig. 4a). Furthermore, reddish intervals of silty sand contrast with grey litharenites (Fig. 4b, d). Between stratigraphic meters 90 and 102 reddish intervals dominate and alternate with few whitish to bright-yellowish horizons (Fig. 4d). We observe the stratigraphic highest reddish horizon at stratigraphic meter 190 m (Fig. 4a). Bad outcrop conditions above sub-section F (> 775 m a.s.l., vegetated and/or inaccessible steep walls) obscured detailed observations. Nevertheless, we found decreasing particle size towards the hanging-wall cutoff line of the Gorno Spanchevo Fault at 915 m a.s.l., implying that sub-section F lacks the top 140 m of deposits. The NE-ward dip of the sediments is 5° at stratigraphic meter 100 and apparently zero above 160 m.

According to the lithostratigraphic subdivision of Kojumdjieva et al. (1982), the lower part of sub-section A corresponds to the Sandanski Formation. The base of the Kalimantsi Formation can be traced with the first coarse conglomerates at stratigraphic meter 30 in sub-section A. The 'red bed unit' corresponds to the Orange and lower Reddish Coarse Fanglomeratic Intervals of sub-sections C, D and F.

4.2. Fossil fauna

Along the Gorna Sushitsa gorge, we identify 14 levels of vertebrate accumulations. The first note on fossil mammals from Gorna Sushitsa gorge was given by Bakalov and Nikolov (1962), but the exact stratigraphic positions of their findings are unknown. Field surveys organized by the National Museum of Natural History in Sofia between 2004 and 2014 identified 16 vertebrate bearing spots (named in order of their discovery GS 1 to GS 16), belonging to 11 stratigraphic levels of

sub-section C (GS 5 and GS 6 crop out in the village Gorna Sushitsa and can not yet be correlated to stratigraphy). In the footwall of the Melnik Fault only the Orange Interval bears fossil bones, the stratigraphically youngest GS 16 is situated at the base of the lowest reddish horizon. The bones appear in mass-accumulations and are dominated by disarticulated large mammal remains. Bones of reptiles and birds are very rare, whereas small mammals and amphibians are lacking.

From the hanging wall of the Melnik Fault, in sub-section A, we found three bone layers (GB 1 to GB 3) in bluish silts within 6 m above the ash layer. In contrast to the GS levels there is no mass accumulation. Instead, large mammal fossils appear preferentially articulated (e.g. limbs bitten by carnivores), and well-preserved small mammals have been found, indicating different taphonomy at both sides of the fault.

4.3. Biochronology

The most diverse fauna from the three GB levels is GB 1, revealing five taxa (the glass lizard *Ophisaurus* sp. and the mammals *Prolagus* sp.,? *Stylocricetus* sp., Rodentia indet., *Propotamochoerus* sp.). The suid *Propotamochoerus*, represented by both hind legs and a lower jaw, belongs to the European late Vallesian-to-Turolian form known from relatively few localities only (van der Made et al., 1999), which are mostly poorly constrained in age (Geraads et al., 2008). However, the latter authors assume that most findings from the Balkans and Turkey belong to the early Turolian.

In GB 1, only few but relatively well-preserved specimens of the pika *Prolagus* are available. Among them, two mandibles show strong size differences, including what concerns the bony part of the mandible (maximum high of the horizontal ramus respectively 8.53 and 5.97 mm), as well as the incisors (width respectively 1.97 and 1.46 mm). Significant differences in tooth size and morphology often reflect the intraspecific or intra-population variability (e.g. López-Martínez, 1989; Angelone and Čermák, 2015). This variability significantly complicates the taxonomic study of reduced fossil samples. This is the case in GB 1. The larger jaw (GPIT/MA/12763 with p3-m1; Fig. 5a and d1) fits metrically with the larger continental *Prolagus* species (p3: 2×2.12 mm), like *P. michauxi* (already mentioned in the Pliocene of Bulgaria, Thomas et al., 1986; but Angelone (2007) questions the presence of the species in eastern Europe), or *P. sorbinii* present in the late Turolian of northern Italy and Greece. Angelone and Čermák (2015) have indeed roughly assigned the latest Miocene southernmost Balkan populations to the *P. sorbinii* group. The morphology of the Gorna Sushitsa p/3 clearly differs from this species and from the latest Turolian premolars from Greece (Maramena, *P. cf. sorbiniide* Bruijn, 1995; Silata and Kessani, *P. michauxi* Vasileiadou et al., 2003, 2012). Although larger, the p/3 from GB 1 recalls in some traits in corresponding teeth from Chomateri (such as *P. cf. crusafonti* in López-Martínez, 1976). Interestingly, the middle Turolian Greek population is characterized by high variability in both size and morphology, some p/3 are very small also lacking the crochet, recalling thus the tooth of the small mandible from Bulgaria (GPIT/MA/12764 with p3-m2; Fig. 5b and d2). This specimen belongs to a very young individual and the length of the p/3 provided herein (1.28×1.61 mm) most probably underestimates the maximum length of the tooth in a later wear stadium. Both mandibles belong to the same species, as well as a fragmentary maxillary (GPIT/MA/12765, Fig. 5c). It lacks unfortunately the P2 but it is relatively large (P3: 1.81×2.92 mm) and conserves a round and small premolar foramen lingual to the mesial hypocone of the P4 which is very different from *P. sorbinii* and *P. michauxi*. Angelone et al. (2014) and Angelone and Čermák (2015) demonstrated the existence of longitudinal gradient in some important morphologic traits in p3, as well as a marked geographic endemism in Europe during the middle and/or late Miocene. The species from GB 1 cannot be clearly included in the Turolian lineage *P. pannonicus*-*P. latincinatus* from Hungary. The early Turolian species from Kohfidisch cannot be compared, because some important morphologic details are

not shown in Bachmayer and Wilson (1970). Similarly, the Turolian species discovered in Ukraine have not been described in details (Čermák et al., 2012). Although sharing some common characteristics, the Bulgarian fossils cannot be assigned with certainty to the middle Turolian *Prolagus* from Moldova (*P. cf. oeningensis* from Rezani in Delinschi, 2014; assignment doubtful for Angelone and Čermák, 2015). As a result, the species from GB 1, possibly new, has to stay in open nomenclature.

A single cricetid mandible preserves the m1 and m2 (GPIT/MA/12766, Fig. 5e). Although this fossil lacks some important morphologic characteristics, the form and division of the anteroconid of the first molar, the lack of mesolophids and the size of the teeth (m1: 2.22×1.26 mm; m2: 1.84×1.44 mm) allow to restrict the comparison to five late Miocene genera. The crown-height is lower than in *Hypso-cricetus*. The metalophulid and hypolophulid are clearly less oblique than in most *Allocricetus* molars. *Pseudocricetus* and *Apocricetus* differ, after Kálin (1999), only in minor details. The species of *Apocricetus* belong to a single lineage (*A. aff. plinii*-*A. angustens*; Ruiz-Sánchez et al., 2014) and none of them show a structure of the anteroconid similar to GB 1. In contrast, it fits with *Pseudocricetus* and the size of the teeth fall in the range of *P. kormosi* and the uppermost size of *P. orienteuropaeus* (see Sinitza, 2010 for comparison). The anterior part of the symphysis ends at about the level of the alveolar process in GB 1, while it ends somewhat deeper in the *Pseudocricetus* mandibles figured by Topachevski and Skorik (1992). This characteristic fits better with *Stylocricetus*, as well as the relatively strong and labially displaced ectostylids that enlarge the posterior parts of the molars, especially the m1. In contrast, the teeth from GB 1 are a bit larger than *S. meoticus*, the only species known to date. Based on the mandible only, any taxonomic assignment remains hazardous, and the fossil is referred to as? *Stylocricetus* sp. One edentulous mandible indicates the presence of a second rodent in the locality.

Stylocricetus is so far known only from the late Miocene of the Ukraine: *Stylocricetus* sp. from Mikhailovka 1 + 2, and Palievo (Nesin and Nadachowski, 2001; Sinitza, 2012), and *S. meoticus* from Cherevichnoé 3, Protopopovka, and Novoelizavetovka 3 (Topachevski and Skorik, 1992). The oldest locality is Mikhailovka 1 at the Bessarabian-Khersonian boundary, the youngest may be Cherevichnoé 3, the bone layer of which is situated 19 m above an erosional unconformity to marine Khersonian sediments and shows a normal magnetic polarity, which is correlated by Vangengeim and Tesakov (2008) to chron C4n. Therefore, the genus *Stylocricetus* may broadly occupy an age range between ~9 and ~8 Ma in the Ukraine, which represents the biochronologic frame provided by the GB 1 mammals.

The large mammal faunas from sub-section C (GS levels) are currently under study. Preliminary taxonomic results indicate, that faunal levels GS3, 7, 9 up to GS16 (between stratigraphic meters 20 to 60) appear rather homogenous from a biochronological point of view, and their species composition are close to the fauna of the classical Pikermi levels (e.g. with *Tragoportax amalthaea* and the Pikermi evolutionary stage of *Mesopithecus pentelicus*). The classical levels of Pikermi date between 7.33 and 7.29 Ma (Böhme et al., 2017). By contrast, the three lower levels GS2, GS12, GS13 (between stratigraphic meters -4 to 6) can be biochronologically discriminated from the younger levels, mainly by more primitive (compared to Pikermi) evolutionary stages of both carnivores *Adcrocuta eximia* and *Paramachaerodus orientalis* found in level GS2 (Spassov et al., 2017).

4.4. Demagnetization and rock magnetic properties

The thermomagnetic experiments show consistent behavior between samples (Fig. 6). In all cases, samples are completely demagnetized at around 580°C, the Curie temperature of magnetite. Chemical alteration (physical removal of magnetic minerals) is suggested from a temperature of 150°C onwards, indicated by reversible behavior transitioning to non-reversible behavior. In general, the thermal properties

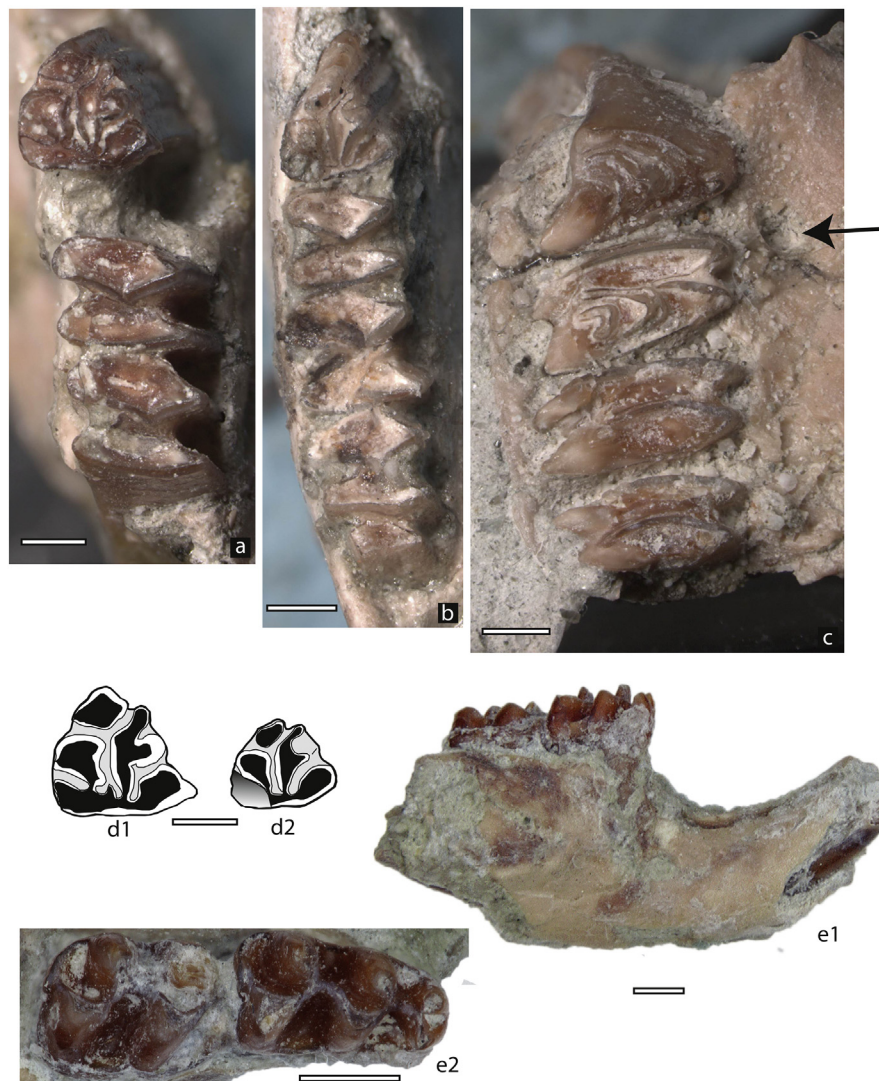


Fig. 5. Small mammals from Gorna Sushitsa, level GB 1. a-d) *Prolagus* sp. a: right mandible with p3-m1 (GPIT/MA/12763). b: right mandible with p3-m2 (GPIT/MA/12764). c: right maxillary with P3-M2 (GPIT/MA/12765). d: drawings of the p3, GPIT/MA/12763 (d1) and GPIT/MA/12764 (d2). Note the black arrow (in c) showing the round and small premolar foramen placed lingual to the mesial hypocone of the P4. e) *Stylocricetus* sp. (GPIT/MA/12766); right mandible with m1-m2 from labial view (e1) and enlargement of the occlusal surface of the teeth (e2). Scales are 1 mm.

are consistent with (detrital) magnetite as the main magnetic carrier.

Thermal demagnetization behavior reflects the observations during the thermomagnetic runs. Most samples show a continuous decrease in intensity up to a maximum temperature of 580–620°C (Fig. 7). During demagnetization, either one, two or three different directional components may be present. A first low temperature (LT) component, if present, is limited to temperatures up to 180–300°C and tends to have normal directions only, which can be interpreted as an overprint of the present-day magnetic field (Fig. 7a). At higher temperatures, a high temperature (HT) component displays both normal and reverse polarities (Fig. 7a,b), which we interpret as the Characteristic Remanent Magnetization (ChRM). Grouping all normal and reverse samples, and running a 45° cut-off, results in two well-defined antipodal mean directions (Fig. 7c). These two mean directions pass the reversal test of McFadden and McElhinny (1988) with a classification B ($\gamma = 4.42$, $\gamma_c = 7.84$). The mean declination of these two directions (359.5° and 180.5° respectively) after removal of the bedding tilt indicates no significant vertical axis rotation has affected the studied record after deposition (see Supplementary Data 2 for all directions).

In a rare case, three unique magnetic directions are observed within the same sample (Fig. 7d,e,f). In this case, in the temperature range

350–480°C a medium temperature (MT) component is present with an antipodal direction compared to the HT direction (Fig. 7d,e). This additional component is clearly apparent in both the vector difference sums and the unblocking spectrum (Fig. 7f). We relate this kind of behavior to delayed acquisition close to a polarity reversal, where the reverse directional component represents the later polarity.

4.5. Magnetic polarity pattern

The three sections at Gorna Sushitsa provide a clear magnetostratigraphy (Fig. 8). The lower half of Section A (46 m) has reverse polarity, except for a single normal polarity sample at 18 m. Above Section A, there is 34 m of normal polarity. Section E has a lowermost 27 m with predominantly normal polarity in which the lowermost 3 m has uncertain polarity. Above the normal, the section has reverse polarity, except for a single sample at 35 m.

Sections B,C,F have a lower 92 m with normal polarity. In this magnetozone, two samples have clear reverse polarity (at –36 m and –14 m). The higher part of the section is dominated by reverse polarities, with a short normal zone at 70–77 m and a slightly longer normal zone of minimum 20 m above stratigraphic level 91 m. The

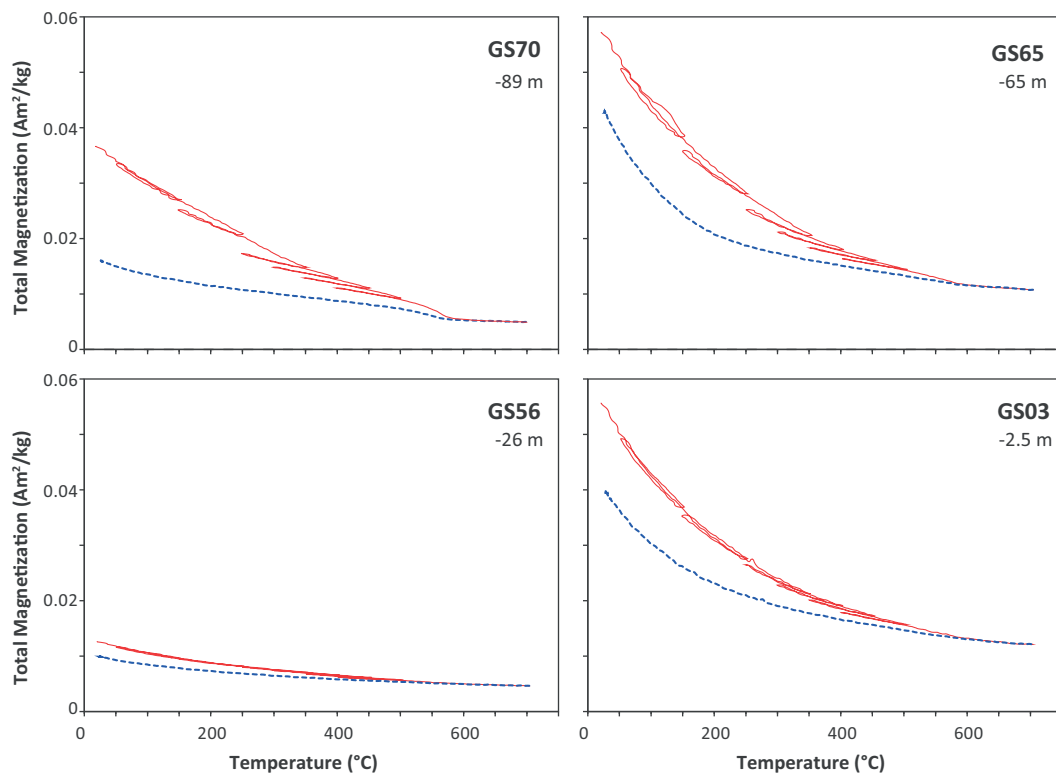


Fig. 6. Typical thermomagnetic behaviour of samples from the studied section. Experiments were carried out by raising temperature to increasingly higher temperatures (red line) up to a maximum temperature of 700 °C. Cooling back to room temperature in blue. (For interpretation of the references to colour in this figure legend, the reader is referred to the web version of this article.)

reversal at the top of this uppermost normal is not present in a continuously sampled section. At the jump from sub-section C to F, a switch of polarity occurs, indicating a small sampling gap may have remained between the two sub-sections. Correlation along strike across the 100% exposed cliff-face between the two sub-sections indicates this gap may be very minor.

4.6. Grain-size data

Fine-clastic sediments of the Orange Interval have fine- to medium-size silt content (4–31 μm) between 12 and 40% (Fig. 9c). Between stratigraphic meter 5–40 in sub-section C, the silt content fluctuates strongly (by up to 25%). We observed the highest silt content (35–40%) during this interval at stratigraphic meters 13, 25, and 33, and lowest values (< 15%) at stratigraphic meters 5, 29, and 37.

From end-member analysis, we identified three robust end-members (EM), whose dominant modes are summarized in Table 1. A linear model based on the three modes explains 83.4% of the total variance in all 34 grain-size spectra (Supplementary Data 1). The medium-silt contribution (EM1, dominant mode 16.7 μm) dominates 11 samples (Fig. 9a) and is characterized by a relatively broad grain-size distribution (EM1gs in Fig. 9b). This distribution comprises the two aeolian end members from the Pikermi Formation (EM1p and EM2p in Fig. 9b) studied in Böhme et al. (2017).

5. Discussion

5.1. Correlation to the Global Polarity Timescale

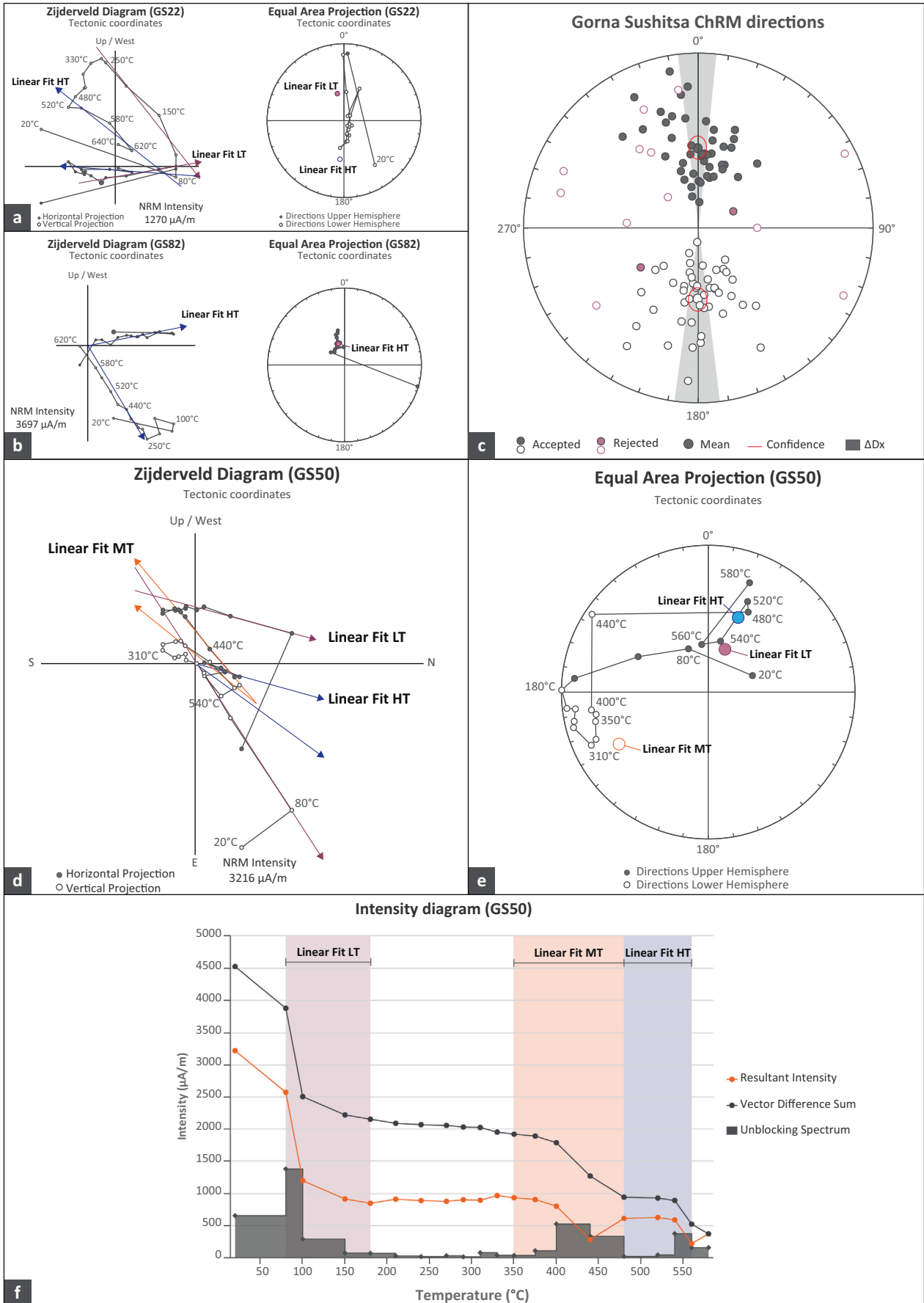
Given the age constraints of the Turolian mammal fauna, a straightforward magnetostratigraphic correlation can be made to the Global Polarity Timescale (GPTS 2012). The GS faunal levels in sub-section C between stratigraphic meters 20 to 60 point to around 7.3 Ma.

Sections B,C,D,F provide a (near-) continuous record from chron C4n.2n to chron C3Ar, representing the time period of ~ 7.8 Ma to ~ 7.0 Ma (Fig. 10). The exact age of the base of this part of the section is unclear, especially because of the presence of the two faults at -40 m and -34 m. The two normal zones between 70 m and 110 m are correlated to chrons C3Br.1n and C3Bn. This implies that the Tortonian-Messinian boundary (7.246 Ma), in the lower part of the reverse chron C3Br.1r, is located at 78 m in sub-section C. The predominance of fine-grained sediment, particularly in this upper part of the section, supports our notion that the average sedimentation rate may have been relatively stable over a longer period.

The magnetostratigraphy of sections A and E can be correlated together, given their close proximity in the lower part of Gorna Sushitsa valley. The available biochronologic data place GB 1 in the early Turolian, approximately at 8 Ma. Unfortunately, the volcanic ash beds in this part of the section were not suitable for $^{40}\text{Ar}/^{39}\text{Ar}$ dating, and could not provide additional age constraints.

The short normal in Section A is correlated to chron C4r.1n at 8.3 Ma. Older correlation options are not likely, given the biochronologic constraints of mammal fauna GB 1 in this normal zone. A younger correlation is not favored as it seems unlikely that this one sample represents the entire chron C4n.2n. The upper part of this section, in which only normal polarities are found for 35 m, can in our preferred correlation be correlated to the lower part of normal chron C4n.2n. This correlation indicates that the section exposes sediments with an age between ~ 8.5 Ma and ~ 8.0 Ma.

Section E stratigraphically overlies Section A, and therefore needs to correlate younger than section A. The predominantly reverse nature of the upper 40 m suggests a correlation to a reverse chron of relatively long duration. The most logical option would in that case be chron C3Br.2r. This implies that the underlying normals correlate to chrons C3Br.2n and C4n.1n, with a potential correlation of the base of the section to the short reverse chron C4n.1r.



(caption on next page)

Fig. 7. Examples of typical thermal demagnetization behaviour. For all subfigures, LT: Low Temperature, MT: Medium Temperature, HT: High Temperature. All directions are presented in tectonically corrected format. a) Zijderveld diagram and equal area plot for a typical, strong reverse magnetized sample (GS22). b) Zijderveld diagram and equal area plot for a typical, strong normal magnetized sample (GS82). c) Determined Characteristic Remanent Magnetization (ChRM) directions for all samples. d,e,f) Example of a sample with three magnetization directions (GS50). d) Zijderveld diagram of sample GS50. e) Equal area projection of sample GS50. f) Intensity diagram of sample GS50, clearly showing three peaks in the unblocking spectrum.

Older correlations of the top reverse to chrons C3Br.3r or C4n.1r cannot fully be excluded, although this is not favored because of the short duration of these chrons. A younger correlation would imply a significant gap to the underlying Section A, which is also not preferred. Our preferred correlation represents the time interval between ~ 7.7 Ma and ~ 7.35 Ma and means that sub-section E should be the time equivalent of the lower to middle part of sub-sections B,C,D,F.

5.2. Implications for lithostratigraphy

In the hanging wall of the Melnik Fault, we observe the superposition of sediments from the Kalimantsi Formation (coarse conglomerates followed by breccias) over Sandanski Formation (coal, silt, sand) in sub-sections A and E. These observations are in agreement with the superposition of the Kalimantsi Formation over Sandanski Formation as supposed by Zagorchev and Dinkova (1990) and Zagorchev (2001). We further confirm the existence of the Red Bed Member (Kojumdgieva et al., 1982), which corresponds to our Orange Interval and the lower part of our Reddish Coarse Fanglomeratic Interval between stratigraphic meters –13 and 102 in sub-section C. In contrast, we cannot confirm the Ilindentsi Member as a stratified unit. Instead, we interpret this marble mega-breccia around the village of Ilindentsi, similar to the situation at the Melnik Fault (Fig. 11), as a syntectonic fault-scarp succession (as also implied by Zagorchev, 1992) of a yet unnamed fault (here: Ilindentsi Fault) in the northern part of the basin between the villages Ilindentsi and Ploski (Fig. 1).

The syntectonic fault-scarp successions along the Melnik and the Ilindentsi faults are composed of huge-clast breccias with catchment-specific components of eroded footwall basement (Fig. 11). Similar granitic or marble mega-breccias are reported from the Serres and Sidirokastro basins, northeastern part of the greater Strymon Basin (e.g. v. Freyberg, 1951; Armour-Brown et al., 1979; Mariolakos et al., 2004; Pimpirev and Beratis, 2010). They are universally interpreted as stratified layers and represent important tie-points in the definitions of lithostratigraphic units, especially the Lefkon ‘formation’ in the Serres Basin (Armour-Brown et al., 1979; Pimpirev and Beratis, 2010). Our results raise serious doubts about the suitability of mega-breccias for lithostratigraphic subdivision, and we suspect they may just as well represent syntectonic fault-scarp successions. The use of breccias as stratigraphic marker horizons creates problems in the correlation of mammalian localities (Armour-Brown et al., 1979; de Bruijn, 1989) and may be responsible for the still controversial stratigraphic and chronologic position of the important locality Maramena (Popov and Neveeskaya, 2000). Further fieldwork is needed to emend the stratigraphy of the greater Strymon Basin.

5.3. Age model for the Kalimantsi Formation and tectonic implications

The Gorna Sushitsa gorge exposes within a nearly 500 m thick section the entire Kalimantsi Formation straddling the Melnik Fault (Fig. 11). Our magnetostratigraphy indicates that this section was deposited within 2 myrs, between 8.5 Ma and 6.5 Ma (Fig. 10). Sedimentation rates calculated from completely recorded magnetic chrons of sub-sections A to E vary between 14 and 41 cm/kyr. We date the base of the Kalimantsi Formation to 8.2 Ma and its top (at the hanging-wall cutoff line of the Gorno Spanchevo detachment) to ~ 6.5 Ma by extrapolation with sedimentation rates from top of sub-section C (29 cm/kyr). Furthermore, we can date the Red Bed Member to between 7.49 and 7.17 Ma, and the youngest reddish horizon in sub-section F to

6.85–6.8 Ma.

Based on this age model we are able to estimate the slip at Melnik Fault. Total fault slip during the last 600 kyrs of activity (7.5 Ma – top chron C4n.1n to 6.9 Ma – cessation of slip) is estimated to 260 ± 10 m, indicating slip rate of 0.43 mm/yr (43 cm/kyr), which is similar to typical long-term slip rates on normal faults (Ravnås and Steel, 1998; Pérouse and Wernicke, 2017). The average slip rate is higher than maximum sedimentation rate, implying the development of a substantial fault scarp during times of Melnik Fault activity (Doglioni et al., 1998). Development of a fault scarp is further supported by the facies variation between sub-section C in the footwall and sub-section E in the hanging-wall.

Our sedimentary logs confirm cyclicity of the Kalimantsi Formation as proposed by Kojumdgieva et al. (1982). The fining-upward to coarsening-upward lithosome (Greyish Interval to Reddish Coarse Fanglomeratic Interval) corresponds to the model suggested for lacustrine synrift successions (Ravnås and Steel, 1998). Accordingly, the Greyish and Bluish Intervals are related to the early stage of rifting, the Orange Interval corresponds to the climax stage, and the lower part of the Reddish Coarse Fanglomeratic Interval to the late stage of rifting. The fining-upward trend observed in the upper Fanglomeratic Interval represents the post-rift stage of tectonic quiescence, confirmed by the horizontal bedding of these youngest deposits. The early rift stage lasts from > 8.5 to 7.5 Ma, the climax stage of fault activity and related subsidence from 7.5 to 7.3 Ma, and the late rift stage from 7.3 to ~ 6.9 Ma. At 6.9 Ma the slip on Melnik Fault and Gorno Spanchevo detachment ceased and deposition of the 180 m thick post rift stage lasts until ~ 6.5 Ma. Our results suggest, in accordance with Kojumdgieva et al. (1982), that the Sandanski Basin infill may represent multiple (two) synrift phases (sensu Ravnås and Steel, 1998, fig. 17). The older phase corresponds to the Delcevo Formation, with the coal-bearing Sandanski Formation as tectonic quiescence package, whereas the younger phase represents the Kalimantsi Formation.

The lack of vertical axis rotation in the palaeomagnetic data from the Kalimantsi Formation (Fig. 7c) suggests that the bulk of extensional exhumation of the SRCC occurred before 8 Ma, during the first two stages of Cenozoic extension from Oligocene till middle Miocene as proposed by Stübner et al. (2016). The late Miocene activation of the West Pirin and Melnik faults have only insignificant contributions to the extension of the northern Aegean region (van Hinsbergen and Schmid, 2012). The end of tectonic activity in the Sandanski Basin at 6.9 Ma is furthermore significantly older than the previously proposed ages within the Pliocene or Quaternary (see Fig. 1). The minor steep faults observed in the Bluish Interval, as well as the similar steeply dipping sparry calcite veins in palaeosols of sub-sections A and E may correspond to short-term Quaternary re-activation of the Melnik Fault, as suggested by Stübner et al. (2016) based on topographic analysis of river channel profiles. This minor and probably short-term re-activation may have also initiated re-sedimentation of fault scarp sediments (‘mega-breccia’) as observed on top of sub-section A (Fig. 3e).

5.4. Biochronologic implications

Based on our age model, we can precisely date the 14 mammal levels found in the Gorna Sushitsa gorge (Table 2), which span a one million year interval within the Tortonian (between 8.3 Ma, mid-Tortonian and 7.3 Ma, latest Tortonian). The precision of the late Tortonian levels is based on the assumption of constant sedimentation rate within the magnetozone that are correlated to chrons C3Br.2r and C3Br.2n

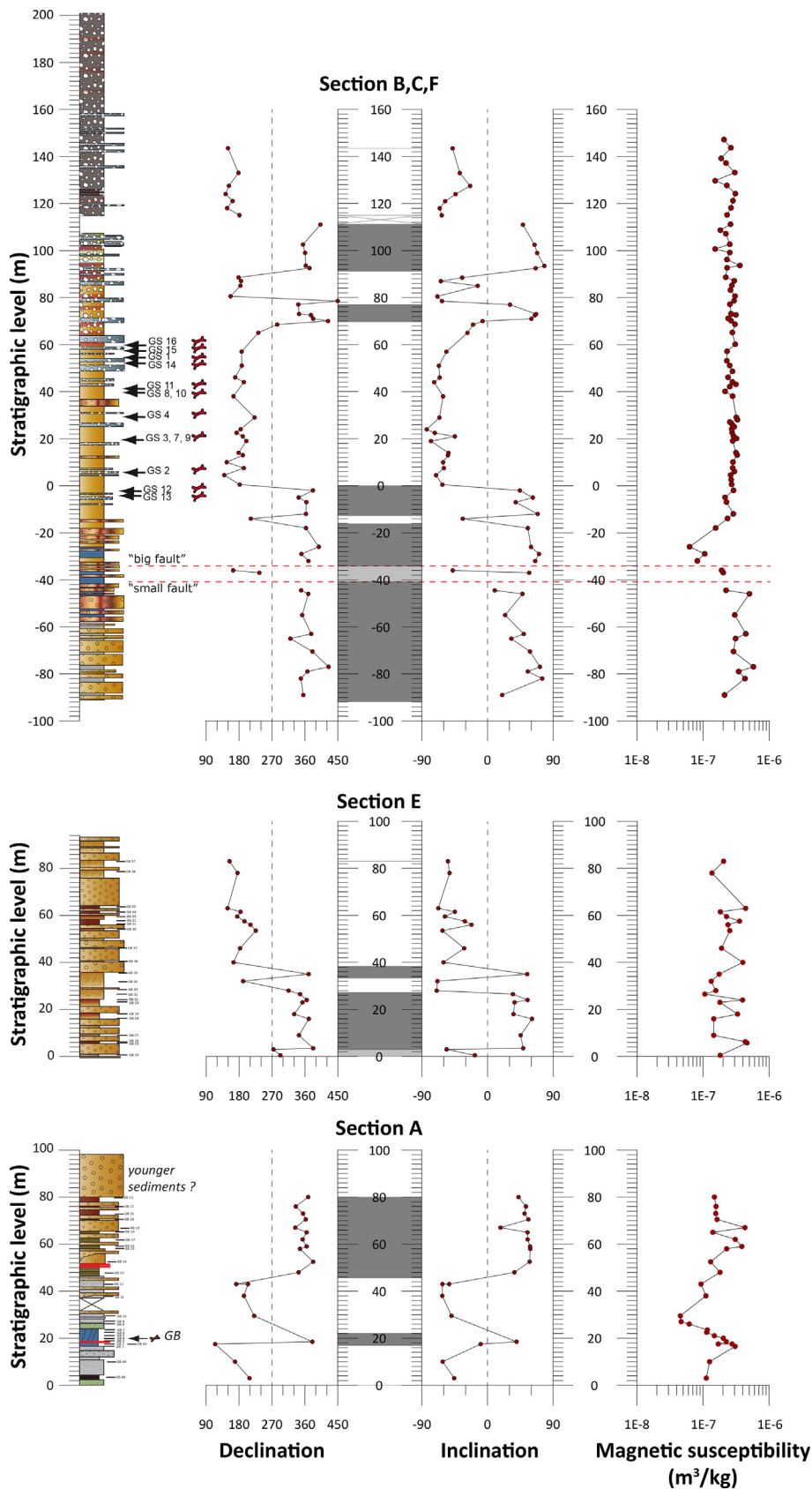


Fig. 8. Magnetostratigraphic results for the three parts of the Gorna Sushitsa section, shown as the declination (horizontal magnetization component), inclination (vertical magnetization component) and the specific magnetic susceptibility (magnetization potential of the material).

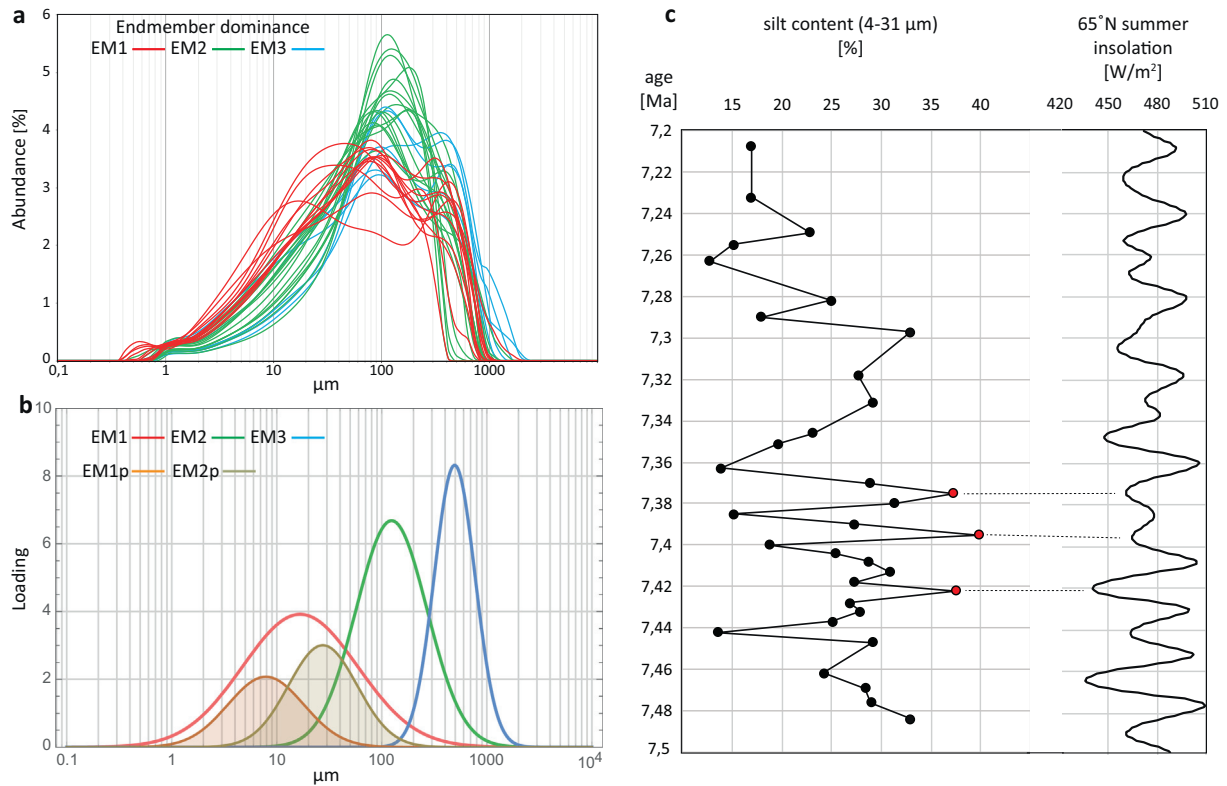


Fig. 9. Grain-size analysis. a) Grain-size distributions (GSD) of 34 samples from Orange and Red Fonglomeratic Intervals. Each GSD is colored according to its dominant end-member. b) Grain-size end-members (EM1, EM2, EM3) found in Gorna Sushitsa samples. The medium-silt contribution in Gorna Sushitsa (EM1) is characterized by a relatively broad distribution and comprises the two silt (aeolian) end members from the Pikermi Formation (EM1p and EM2p) studied in Böhme et al. (2017). c) Chronologic distribution of each Gorna Sushitsa sample according to our age-model plotted against silt content (4–31 μm). Samples with over 70% explained variance of aeolian EM1 (red dots) showing highest silt content and correlate to 65° N summer insolation minima (Laskar et al., 2004). (For interpretation of the references to colour in this figure legend, the reader is referred to the web version of this article.)

Table 1

Sediment components obtained by end-member (EM) analysis of 34 samples from sub-section C in Gorna Sushitsa gorge. The dominant modes were fitted with a normal distribution in Φ -units with mean (x_{mod}) and standard-deviation σ_x . The variance of each EM is expressed relative to the total explained variance.

EM	Particle size class	Dominant modes			Var. Expl. [% of Tot]
		x_{mod} [μm]	x_{mod} [Φ]	σ_x [Φ]	
1	medium silt	16.7	5.90	1.82	37.0%
2	very fine sand	124	3.01	1.13	36.0%
3	coarse sand	494	1.02	0.65	10.4%

(see also discussion in next chapter on orbital driven dust deposition). This part of the section is predominantly fine-grained, with coarser conglomerates and fonglomerates forming a minor lithological contribution. As such, we feel reasonably confident that sedimentation rate did not vary too much across this interval. Individual ages may have an internal error in the order of thousands of years.

A change in the stage of evolution of the carnivores *Adcrocuta eximia* and *Paramachaerodus orientalis* (Spassov et al., in press) between faunal level GS2 (7.44 Ma) and the stratigraphically higher level GS3, 7, 9 (7.41 Ma) is remarkable and may be interpreted to represent the early-to-middle Turolian transition. If true, this boundary can be placed at 7.42 Ma (lower part of C3Br.2r), which is younger than proposed by Agusti et al. (2001) and Van Dam (2001) (within chron C4n.1n, 7.58 Ma), or Kostopoulos et al. (2003) (boundary C3B/C4n, 7.64 Ma).

A Middle Turolian fauna composition, very much comparable to the classical Pikermi, appears between 7.41 and 7.31 Ma (faunal level GS3,

7, 9 up to level GS16). The Pikermian middle Turolian fauna is characterized by the dominance of hipparionine horses (*Hippotherium brachypus*, *Cremohipparion mediterraneum*), gazelles, spiral-horned bovinds and boselaphins (*Gazella*, *Protragelaphus*, *Prostrepsiceros*, *Tragoportax amalthea*), the co-occurrence of at least two giraffid (*Palaeotragus rouenii*, *Bohlinia attica*) and two rhino species (*Ceratotherium neumayri*, *Dihoplus pikermiensis*) with the colobine monkey (*Mesopithecus penelicus* s.str.), and the advanced evolutionary stages of the hyaena and the felid *Adcrocuta eximia* and *Paramachaerodus orientalis* (Spassov et al., 2004; Geraads et al., 2006, 2011; Geraads and Spassov, 2009; Koufos, 2009; Roussiakis, 2009; Theodorou et al., 2010; Kostopoulos and Bernor, 2011; Spassov et al., in press). In Pikermi, these associations are found until 7.27 Ma (Böhme et al., 2017), indicating that the Pikermian type fauna has a short duration of 150 kyrs only. A significant faunal turnover at the Tortonian-Messinian boundary brings new immigrants (e.g. the elephantid *Anancus*, the boselaphid *Tragoportax macedonensis*, the potential hominin *Graecopithecus freybergi*) into the Balkans, referred as the post-Pikermi fauna (Spassov et al., 2012; Böhme et al., 2017).

Our results also allow geochronologic assessment of the important SW-Bulgarian faunas of Kalimantsi (Sandanski Basin) and Hadjidimovo (Mesta Basin), both localities without stratigraphic control. Based on the stage-in-evolution of their large mammals (Spassov, 2002; Spassov et al., 2006; Li and Spassov, 2017) Hadjidimovo and Kalimantsi 1 should be older than 7.44 Ma, whereas the localities Kalimantsi 2 and Kalimantsi 4 can be correlated to the middle Turolian, in the time interval 7.42–7.27 Ma.

5.5. Palaeoenvironment during the deposition of the Kalimantsi formation

The presence of a significant fault scarp during synrift deposition

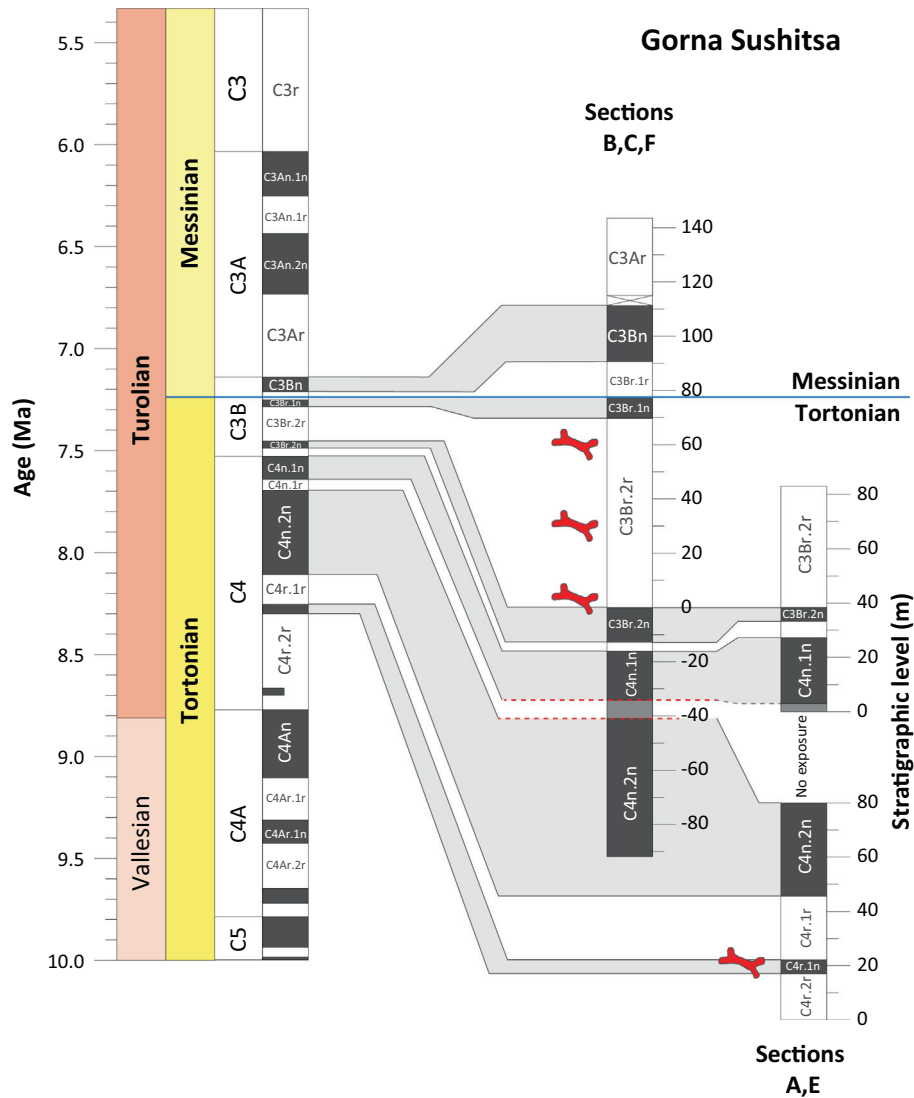


Fig. 10. Correlation of the three parts of the composite section to the Global Polarity Time Scale (GPTS 2012). Sections A and E are separated from sections B,C,F by the tectonic breccia representing the Melnik Fault. Solid correlation lines indicate position of magnetic reversals, dashed lines the approximate correlation of the base of the sections.

along the Melnik Fault implies different palaeoenvironments in its hanging wall and footwall. On the footwall, where the Pikermian mammal accumulations occur, slopes are steeper and experienced faster runoff with well-drained but poorly developed soils. The dominance of

fanglomerates and the lack of larger rhizoliths may indicate relatively open environments (scrublands), consistent with the occurrence of the soil bee ichnofossil *Celliforma*, characterizing well-drained soils under low vegetation cover (Genise et al., 2010; Cardonatto et al., 2016). In

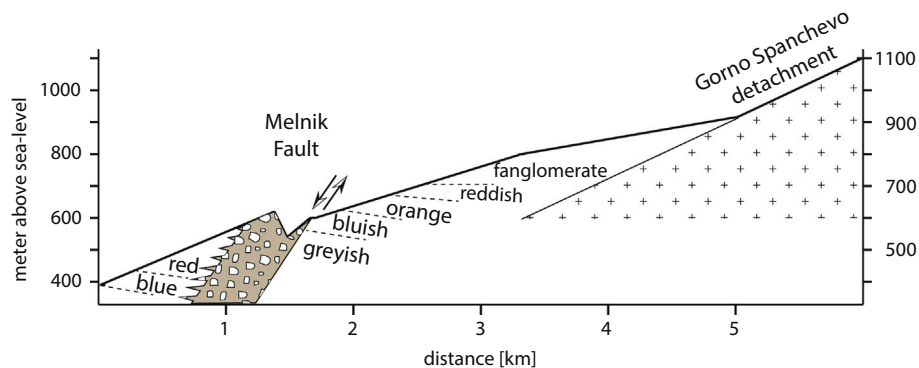


Fig. 11. Southwest-northeast transect through the Gorna Sushitsa gorge (see Fig. 2) showing the sedimentary units, the syntectonic megabreccia of the Melnik Fault and the onlap of deposits on the Gorno Spanchevo detachment.

Table 2
Magnetostratigraphic dating (GPTS2012) of mammalian levels in the Gorna Sushitsa gorge and comparison with dated mammal levels from Pikermi (Böhme et al., 2017).

Gorna Sushitsa	Age (Ma)	Pikermi	Age (Ma)
GS 16	7,31	PV1	7,28 - 7,27
GS 15	7,315	PV3 upper levels	7,31 - 7,29
GS 1	7,32		
GS 14	7,33	PV3 lower level	7,33
GS 11	7,355		
GS 8, 10	7,36		
GS 4	7,38		
GS 3, 7, 9	7,41		
GS 2	7,44		
GS 12	7,46		
GS 13	7,47		
GB 3	8,25		
GB 1	8,27		
GB 2	8,3		

contrast, in the hanging wall slopes are flatter and run-off is less erosive. This latter environment was more stable, which becomes apparent by well-developed palaeosols (Fig. 3e), the preservation of thin ash-layers, and minor contributions of fanglomerates, relative to the foot-wall. Large rhizoliths are similarly absent indicating open environment as well. These observations fit very well with the large mammals of Pikermian type observed in sub-section C (see above, and Spassov, 2002; Spassov et al., 2006 for detailed faunal analysis and interpretations).

5.6. Palaeoclimate

The lithological composition and the mode of sediment deposition can be interpreted in terms of local and supra-regional climatic

developments (Fig. 12). The upper part of Sandanski Formation is characterized by organic-rich coaly horizons, representing lacustrine-to-marsh facies, and fine-to-coarse grained fluvial sediments with greenish-greyish overbank deposits (Fig. 3d, g). This pattern reflects moderately humid conditions from 8.5 to 8.2 Ma. At the onset of the Kalimantsi Formation at 8.2 Ma the climate is dryer, reflected by well-oxygenized overbank sediments with rubified upper soil horizons (Fig. 3e, f). Relatively dry climate prevails during the Greyish Interval, with rubified soils in sub-section B and unsorted sub-angular debris in sub-section C, up to 7.8 Ma (at stratigraphic meter –56 in sub-section C). The following Bluish Interval indicates reduced oxygenation of overbank sediments, interpreted as increase in humidity. Humidity is high during the upper part of Bluish Interval between 7.74 Ma and 7.56 Ma (stratigraphic meters –47 to –26 in sub-section C), as reflected by the dominance of conglomerates over fanglomerates. The Transitional Interval (7.56–7.49 Ma) shows an increase in unsorted breccia-conglomerates, which indicate a transition towards arid climate. Aridization starts with the beginning of the Orange Interval at 7.49 Ma, indicated by beginning predominance of fanglomerate layers and cessation of fluvial conglomerates (last conglomerate at 7.365 Ma at stratigraphic meter 36 in sub-section C). The interpretation of local climate developments in younger parts of the section is obscured by the dominance of breccias during the late rift stage and the proximal position of sub-section F to the Gorno Spanchevo detachment.

Information on supra-regional climate trends can be gained by analyzing potential contributions of aeolian dust admixture. As revealed by Böhme et al. (2017), the latest Tortonian to early Messinian (7.4 to 6.9 Ma) was a time of intense dust production over Northern Africa, and significant reddish peri-desert loess deposits accumulate at the northern fringe of the Western and Eastern Mediterranean. Earliest Messinian dust deposition reaches northward at least to 42° latitude in the Upper Thracian Basin, where dust represents an important component of palaeosols of the Ahmatovo Formation in Azmaka (Böhme et al.,

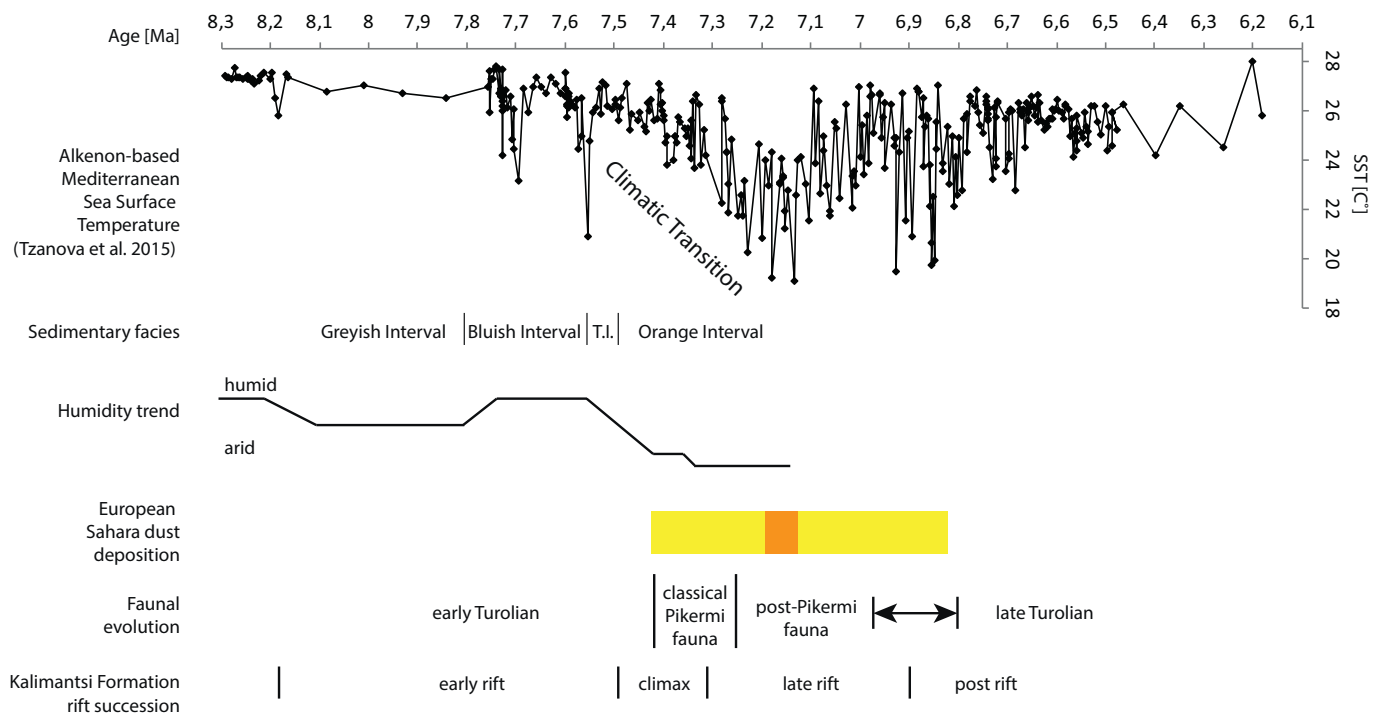


Fig. 12. Tortonian-Messinian climate and Turolian mammals in the Balkan Peninsula. Synopsis of a) global (alkenone-based Mediterranean Sea Surface Temperature, SST, Tzanova et al., 2015), b) local (sedimentary facies of Kalimantsi Formation), c + d) regional (c – humidity trend Sandanski Basin; d – mammal chronologic subdivision in the Balkans), and e) supra-regional (yellow - Sahara-born dust deposition in Europe; orange – climax of earliest Messinian Sahara desertification according to Böhme et al., 2017) events during the late Tortonian and early Messinian. (For interpretation of the references to colour in this figure legend, the reader is referred to the web version of this article.)

2017). In Gorna Sushitsa, the medium-silt dominated end-member in the grain-size distribution (EM1gs, dominant mode 16.7 μm) comprises both aeolian end-members of the contemporary Pikermi Formation in Attica (dominant mode EM1p 7.9 μm , EM2p 27.4 μm), suggesting that EM1 in Gorna Sushitsa originates from Sahara dust as well (Fig. 9b). Based on our age model we display the dust related fine- to medium-size silt content (Vandenbergh, 2013) of the Orange Interval in chronologic frame (Fig. 9c). Between 7.44 and 7.36 Ma silt content shows high amplitude fluctuations at high frequency at about precession scales. The match to the orbital target curve is not perfect, because our dust samples have a mean temporal resolution of only 6.5 kyrs during C3Br.2r, and our age model assumes constant rates of sedimentation (41 cm/kyr during chron C3Br.2r), which is rather unrealistic at shorter time scales of few thousand years. Furthermore, a short time-lag between insolation minima and onset of dust deposition seems possible.

Nevertheless, most maxima and minima of silt accumulation correlate well with minima, respectively maxima of northern 65° summer insolation. Larrasoana et al. (2003) have documented the same phase relation in Plio-Pleistocene marine dust records from the Eastern Mediterranean and relate dust minima to northward penetration of the African summer monsoon front during insolation maxima. Accordingly, we interpret high fine- to medium-silt content during the Orange Interval, especially the three maxima at 7.422, 7.395, and 7.375 Ma as periods of enhanced Saharan dust accumulation. This extends onset of the late Tortonian dust record from Pikermi in Attica (limited there by outcrop conditions to 7.37 Ma) by 50 kyrs. The grain-size based dust signal is obscured in the upper part of the Orange Interval and in the Reddish Coarse Fanglomeratic Interval due to rift-related successive coarsening of sediments (see above). However, the characteristic ~2 m thick reddish horizons (Fig. 4 b, d) occur in sub-section F up to stratigraphic meter 190, suggesting recurrent dust deposition until 6.85–6.8 Ma. This upper end of dust deposition matches the youngest dust record from Attica (top of Rafina Formation) dated to 6.9 Ma (Böhme et al., 2017).

Whereas the northern fringe of the Mediterranean Sea experienced massive loess deposition (e.g. at Pikermi and Pyrgos Vassilissis in Attica, Greece; at Mont Luberon in Vaucluse, France; Böhme et al., 2017), dust in the more central parts of the Balkan Peninsula (Sandanski Basin, Upper Thrace Basin) provides only a silty admixture to soil systems. This observed Miocene pattern matches well the present-day European dustfall regions as defined by Stuut et al. (2009).

Recently, Palcu et al. (2018) propose palaeo-humidity trends for the Eastern Paratethys based on magnetostratigraphic dating of Khersonian and Maeotian sediments and inferred lake level fluctuations in the Dacian Basin. They date the Eastern Paratethyan lake level low-stand during the late Khersonian (Kojumdjieva, 1983), and hence the dry Khersonian conditions, to 8.6–7.65 Ma. The Maeotian transgression is found to be diachronous in the Dacian Basin between 7.65 and 7.4 Ma. Palcu et al. (2018) explain this stepwise flooding of marginal basins by a change to positive water balance, and hence humid conditions, in the Paratethys region. This interpretation is partly supported by our data. The younger humid period in our Sandanski record lasted from 7.8 to 7.49 Ma (Bluish and Transitional Intervals), with peak humidity from 7.74–7.56 Ma (Fig. 12). This period can potentially be responsible for the shift of the Paratethyan water budget leading to the Maeotian transgression. Our data further suggest that the late Khersonian dry period (8.6–7.65 Ma, Palcu et al., 2018) contains an interval of reduced aridity between 8.5 and 8.2 Ma (upper part of Sandanski Formation). Most importantly, our Sandanski record reveals a trend of increasing aridity after 7.49 Ma, which seems not reflected in the Dacian Basin lake level record.

5.7. The Pikerimian event and global climate changes during the latest Tortonian

A proposed middle Tortonian transgression of the Mediterranean into northern Greece and hence the formation of the Aegean Sea is critical in the biogeographic model explaining the Pikerimian Event (Kostopolous, 2009). Von Freyberg (1951), who described a bank of reef corals associated with normal marine bivalves directly northeast of Serres (Strimon Basin), first recognized late Miocene marine transgression from the Mediterranean into the north Aegean realm. This bed has later been included into the Dafni Formation by Gramann and Kockel (1969). The top of the marine Dafni Formation is dated by U–Pb geochronology on zircons from an ash layer at the base of the overlying brackish (Paratethyan) Choumnikon Formation to 6.1 Ma (Grossi et al., 2015), which compares to magnetostratigraphic dating of this transition to 6.3 Ma (Snel et al., 2006). The base of the Dafni Formation, the transgression itself, is less clear. Snel et al. (2006) propose an early Messinian transgression based on calcareous nannoplankton of zone NN11b from sediments correlating to chron C3An.2n. We therefore conclude that there is no evidence for a Tortonian transgression in this area and that the Aegean Sea, as a significant biogeographic barrier between the southern Balkans and Anatolia, was established just during the early Messinian.

The reasons for the increased early Turolian mammal faunal inhomogeneity between the Balkan and Anatolia should therefore have different reasons. The observed homogenization of the Balkan and Anatolian faunas (the Pikerimian Event of Kostopolous, 2009) may instead be provoked by global climate change (Fig. 12). The temporal window of the Pikerimian fauna (7.42 and 7.27 Ma) is characterized by the first glaciations of southern Greenland (St. John and Krissek, 2002) and cooling of the Southern Ocean water masses (Billups, 2002), leading also to significant mid-latitude oceanic cooling (Herbert et al., 2017). Sea-surface temperatures in the Mediterranean (Tzanova et al., 2015) drop stepwise up to 9 °C (Fig. 12), and desertification of North Africa and probably Arabia (Böhme et al., 2017) may have triggered mammalian dispersal from the eastern Mediterranean (Anatolia, Iran) towards the West, where suitable habitats persisted for the savannah-like large mammal association, despite an increasingly dry Balkan area (Fig. 12).

6. Conclusions

The Sandanski Basin infill (third Cenozoic extension of Stübner et al., 2016) represents two stacking synrift phases. The older phase correspond to the Delcevo Formation, which is still magnetostratigraphically undated. The coal-bearing Sandanski Formation represents the tectonic quiescence package, whereas the younger synrift phase, including the post-rifting deposits, is identified as the Kalimantsi Formation. In the 500 m thick sedimentary sequence of the Gorna Sushitsa gorge, we observe superposition of Sandanski and Kalimantsi formations. Palaeomagnetic and biochronologic investigation enables a straightforward magnetostratigraphic correlation to the Late Miocene chrons C4r.2r to C3Ar of the Global Polarity Timescale. The duration of sedimentation of the studied sections is 2 myrs, between 8.5 and 6.5 Ma (late Tortonian to early Messinian). The transition of the Sandanski to Kalimantsi Formation is dated at 8.2 Ma and post-rifting deposits of Kalimantsi Formation to between 6.9 and 6.5 Ma. The younger synrift phase (8.2–6.9 Ma) shows high subsidence rates during the latest Tortonian. Post-rifting deposition starts with the cessation of slip on Melnik and Gorno Spanchevo Faults at 6.9 Ma, probably caused by a switch from regional E–W to N–S extension between 7 and 6.5 Ma. Only the Melnik Fault was briefly re-activated during the Quaternary. The average slip rate at Melnik Fault is found to be higher than maximum sedimentation rates, inducing the development of a substantial fault scarp during the younger synrift phase. Syntectonic fault-scarp succession appears on major intra-basinal faults (Melnik Fault, Ilindentsi

Fault) and create mega-breccias composed of local lithologies from the catchment. Such mega-breccias are unsuitable for lithostratigraphic subdivision in the Sandanski basin and their use in the nearby greater Strymon Basin has to be reconsidered.

Sedimentary and faunal characteristics indicate significant climatic fluctuations, especially with respect to humidity. Moderate humid conditions prevail 8.5–8.2 Ma, followed by relatively dry period from 8.2 to 7.8 Ma. We reconstruct a second humid interval from 7.74–7.56 Ma and subsequent significant aridization. This second humid interval may be responsible for a switch in the water budget of the late Khersonian Paratethys lake, causing a step-wise Maeotian transgression as proposed by Palcu et al. (2018). Supra-regional aridization is indicated in our Sandanski record by the onset of reddish silt deposition at 7.42 Ma, interpreted as Sahara-born aeolian dust deposition as described from contemporary northern Mediterranean deposits. Amplitude variations of fine and medium silt content suggest that Sahara dust production is orbital driven. Its deposition in the Sandanski Basin can be traced for at least 600 kyrs, from 7.42 to 6.85–6.8 Ma. This late Tortonian climate change leads to considerable environmental and faunal change in the Eastern Mediterranean and beyond (e.g. Liu et al., 2016). Open environment prevails during the studied interval, and between faunal levels GS2 (7.44 Ma) and level GS3, 7, 9 (7.41 Ma) we observe changes in state of evolution of certain carnivore species (*Adcrocuta eximia*, *Paramachaerodus orientalis*). The strong faunal homogenization in the Balkans and Anatolia during the Pliocene times (described as the ‘Pliocene Event’ by Kostopoulos, 2009) are according to our data rather driven by global cooling and mid-latitude desertification, than by palaeogeographic changes. We date the Pliocene type fauna in Bulgaria and Greece to between 7.42 and 7.27 Ma, indicating that this traditional middle Turolian association is of short duration (150 kyrs) only.

Acknowledgement

We thank Denis Geraads (Paris), Tzanko Tzankov (Blagoevgrad), and August Ilg (Düsseldorf) for joint field campaigns, and especially the local people from Gorna Sushitsa for their hospitality and important help. We further thank Konstanze Stüber (Potsdam) and two anonymous reviewer for critical reading of the manuscript and Agnes Fatz (Tübingen) for grain-size measurements. JP thanks Chiara Angelone (Rome) for kind discussions regarding the taxonomic assignment of the *Prolagus* specimens. Financial support was provided by the German Science Foundation (DFG), grant number BO1550/19-1.

Appendix A. Supplementary data

Supplementary data to this article can be found online at <https://doi.org/10.1016/j.gloplacha.2018.07.019>.

References

- Agusti, J., Cabrera, L., Garcés, M., Krijgsman, W., Oms, O., Parés, J.M., 2001. A calibrated mammal scale for the Neogene of Western Europe. *State of the art. Earth Sci. Rev.* 52, 247–260.
- Angelone, C., 2007. Messinian Prolagus (Ochotonidae, Lagomorpha, Mammalia) of Italy. *Geobios* 40, 407–421.
- Angelone, C., Čermák, S., 2015. Two new species of Prolagus (Lagomorpha, Mammalia) from the late Miocene of Hungary: taxonomy, biochronology, and palaeobiogeography. *Paläontol. Z.* 89, 1023–1038.
- Angelone, C., Prieto, J., Gross, M., 2014. Complement to the study of the pikas (Lagomorpha, Ochotonidae) from the middle Miocene of Gratkorn, Austria. *Palaeobiodiversity Palaeoenvironments* 94, 125–134.
- Armour-Brown, A., de Bruijn, H., Maniati, C., Siatos, G., Niesen, P., 1979. The geology of the Neogene sediments north of Serrai and the use of rodent faunas for biostratigraphic control. In: *Proceedings of the 6th Colloquium on the Geology of the Aegean Region*, Athens. vol. 1977(2). pp. 615–622.
- Bachmayer, F., Wilson, R.W., 1970. Die Fauna der altpliozänen Höhlen- und Spaltenfüllungen bei Kohfidisch, Burgenland (Österreich). Small Mammals (Insectivora, Chiroptera, Lagomorpha, Rodentia) of the Kohfidisch Fissures of Burgenland, Austria. *Ann. Naturhist. Mus. Wien* 74, 533–587.

- Bakalov, P.N., 1933. Localities of Hipparion fauna in Sweti Wrac region. *Rev. Bulg. Geol. Soc.* 5 (3), 257–260 (in Bulgarian).
- Bakalov, P.N., 1934a. Die Hipparionfauna von Kalimanci und Kromidovo, Bezirk Sweti Wrac, SW Bulgarien. (I. Fissipedia und Suidae). *Annuaire de l'Université de Sofia Faculté de Physique-Mathématique* 30 (3), 313–349 (in Bulgarian with German summary).
- Bakalov, P.N., 1934b. Die Hipparionfauna von Kalimanci und Kromidovo, Bezirk Sweti Wrac, SW Bulgarien. (II. Primates – Anthropoidea, Cynopithecidae). *Geol. Balkanica* 1 (1), 17–24 (in Bulgarian with German summary).
- Bakalov, P.N., 1939. Die Hipparionfauna von Kalimanci und Kromidovo, Bezirk Sweti Wrac, SW Bulgarien. (III. Rhinocerotidae). *Geol. Balkanica* 3 (2), 82–88 (in Bulgarian with German summary).
- Bakalov, P.N., 1953. Die Hipparionfauna von Kalimanci und Kromidovo, Bezirk Sandanski, SW Bulgarien. (IV. Artiodactyla, Selenodontia). *Izvestia Geol. Inst. Bulg. Acad. Sci.* 2, 88–125 (in Bulgarian with German summary).
- Bakalov, P., Nikolov, I., 1962. Les fossiles de Bulgarie. X. Mammifères tertiaires. *Acad. Sci. Bulgarie* 162 (in Bulgarian, with French and Russian summaries).
- Billups, K., 2002. Late Miocene through early Pliocene deep water circulation and climate change viewed from the sub-Antarctic South Atlantic. *Palaeogeogr. Palaeoclimatol. Palaeoecol.* 185, 287–307.
- Böhme M, Spassov N, Ebner M, Geraads D, Hristova L, Kirscher U, Kötter S, Linnemann U, Prieto J, Roussiakis S, Theodorou T, Uhlir G, Winklhofer M. (2017) Messinian age and savannah environment of the possible hominin Graecopithecus from Europe. *PLoS One* 12(5): e0177347. <https://doi.org/10.1371/journal.pone.0177347>.
- de Bruijn, H., 1989. Smaller mammals from the upper Miocene and lower Pliocene of the Strimon basin, Greece. Part 1. Rodentia and Lagomorpha. *Bollettino della Società Paleontologica Italiana* 28 (2–3), 189–195.
- de Bruijn, H., 1995. The vertebrate locality Maramena (Macedonia, Greece) at the Turolian-Ruscian boundary (Neogene) 11. *Lagomorpha. Münchner Geowissenschaftliche Abhandlungen A* 28, 133–136.
- Burchfiel, B.C., Nakov, R., Tzankov, T., Royden, L.H., 2000. Cenozoic extension in Bulgaria and northern Greece: the northern part of the Aegean extensional regime. *Geol. Soc. Lond. Spec. Publ.* 173 (1), 325–352.
- Burchfiel, B.C., Nakov, R., Tzankov, T., 2003. Evidence from the Mesta half-graben, SW Bulgaria, for the late Eocene beginning of Aegean extension in the Central Balkan Peninsula. *Tectonophysics* 375 (1), 61–76.
- Cardonatto, M.C., Sostillo, R., Visconti, G., Melchor, R.N., 2016. The Celliforma ichnofacies in calcareous paleosols: an example from the late Miocene Cerro Azul formation, La Pampa, Argentina. *Palaeogeogr. Palaeoclimatol. Palaeoecol.* 443, 203–215.
- Čermák, S., Angelone, C., Rekovets, L., 2012. The Late Miocene–Pliocene Prolagus of Central and Eastern Europe. In: *The 4th World Lagomorph Conference, Volume of Abstracts* 36, Vienna, Austria.
- Delinschi, A., 2014. Late Miocene lagomorphs from the Republic of Moldova. *Ann. Paléontologie* 100, 157–163.
- van der Made, J., Krakhmalnaya, T., Kubiak, H., 1999. The pig Propotamochoerus palaeochoerus from the upper Miocene of Grytsiv, Ukraine. *Estudios Geol.* 55, 283–292.
- Dietze, M., Dietze, E., 2013. A flexible open-source toolbox for robust end-member modelling analysis-The Rpackage EMMAgeo. In: *EGU General Assembly Conference Abstracts* 2013, pp. 2779.
- Dinter, D.A., 1998. Late Cenozoic extension of the alpine collisional orogen, northeastern Greece: origin of the North Aegean basin. *Geol. Soc. Am. Bull.* 110, 1208–1230.
- Dogliani, C., D'Agostino, N., Mariotti, G., 1998. Normal faulting vs regional subsidence and sedimentation rate. *Mar. Pet. Geol.* 15, 737–750.
- Drenovski, K., 1932. First find of monkey remains in Bulgaria. *Priroda i Nauka* 3, 46 (in Bulgarian).
- Freyberg, G.v., 1951. Geologie und Lagerstättenkunde des Braunkohlenreviers von Serrai (Makedonien). *Ann. Geol. Pays Helleniques* 3, 87–154.
- Fuss, J., Spassov, N., Begun, D.R., Böhme, M., 2017. Potential hominin affinities of Graecopithecus from the late Miocene of Europe. *PLoS One* 12 (5), e0177127.
- Genise, J.F., Melchor, R.N., Bellosi, E.S., Verde, M., 2010. Invertebrate and vertebrate trace fossils in carbonates. In: *Alonso-Zarza, A.M., Tanner, L. (Eds.), Carbonates in Continental Settings. Developments in Sedimentology*, vol. 61. Elsevier Publishing Group, Amsterdam, pp. 319–369.
- Geraads, D., Spassov, N., 2009. Rhinocerotidae (Mammalia) from the late Miocene of Bulgaria. *Palaeontographica A* 287 (4–6), 99–122.
- Geraads, D., Spassov, N., Kovachev, D., 2006. A new *Sporadotragus* (Bovidae, Mammalia) from the late Miocene of Bulgaria. *Riv. Ital. Paleontol. Stratigr.* 112 (3), 473–479.
- Geraads, D., Spassov, N., Garevski, R., 2008. New specimens of Propotamochoerus (Suidae, Mammalia) from the late Miocene of the Balkans. *N. J. Geol. Palaont. Abh.* 248, 103–113.
- Geraads, D., Spassov, N., Hristova, L., Markov, G.N., Tzankov, T., 2011. Upper Miocene mammals from Strumyani, south-western Bulgaria. *Geodiversitas* 33 (3), 451–484.
- Gramann, F., Kockel, F., 1969. Das Neogen im Strimonbecken (Griechisch-Ostmakedonien). I - Lithologie, Stratigraphie und Paläogeographie. *Geologisches Jahrbuch* 87, 445–484.
- Grossi, F., Faranda, C., Cosentino, D., Gliozzi, E., Bowring, S.A., 2015. Late Miocene Mediterranean-Paratethys connection: new evidence from the ostracod fauna of the Strymon Basin (northern Greece). In: *Perrier, V., Meidla, T. (Eds.), Abstracts, 8th European Ostracodologists' Meeting. Tartu, Estonia, 22-30 July 2015. Tartu, 2015*, pp. 29.
- Herbert, T.D., Lawrence, K.T., Tzanova, A., Peterson, L.C., Cabellero-Gill, R., Kelly, C.S., 2016. Late Miocene global cooling and the rise of modern ecosystems. *Nature Geosci.* <https://doi.org/10.1038/NNGEO2813>.
- van Hinsbergen, D.J.J., Schmid, S.M., 2012. Map view restoration of Aegean–west Anatolian accretion and extension since the Eocene. *Tectonics* 31, TC5005. <https://doi.org/10.1029/2012TC003132>.

- Kälin, D., 1999. Tribe Cricetini. In: Rössner, G., Heissig, K. (Eds.), *The Miocene Land Mammals of Europe*. Verlag Dr.Pfeil, Munich, pp. 373–387.
- Kojumdjieva, E., 1983. Palaeogeographic environment during the desiccation of the Black Sea. *Palaeogeogr. Palaeoclimatol. Palaeoecol.* 43, 195–204.
- Kojumdjieva, E., Nikolov, I., Nedialkov, P., Buzev, A., 1982. Stratigraphy of the Neogene in Sandanski graben. *Geol. Balcanica* 12 (3), 69–81.
- Konert, M., Vandenberghe, J., 1997. Comparison of laser grain size analysis with pipette and sieve analysis: a solution for the underestimation of the clay fraction. *Sedimentology* 44 (3), 523–535.
- Kostopoulos, D.S., 2009. The Pliocene event: temporal and spatial resolution of the Turolian large mammal fauna in SE Europe. *Palaeogeogr. Palaeoclimatol. Palaeoecol.* 274, 82–95.
- Kostopoulos, D.S., Bernor, R.L., 2011. The Maragheh bovids (Mammalia, Artiodactyla): systematic revision and biostratigraphic-zoogeographic interpretation. *Geodiversitas* 33 (4), 649–708.
- Kostopoulos, D.S., Sen, S., Koufos, G.D., 2003. Magnetostratigraphy and revised chronology of the late Miocene mammal localities of Samos, Greece. *Int. J. Earth Sci. (Geol. Rundsch.)* 92, 779–794.
- Koufos, G., 2009. The genus *Mesopithecus* (Primates, Cercopithecidae) in the late Miocene of Greece. *Bollettino della Società Paleontologica Italiana* 48 (2), 157–166.
- Kounov, A., Wüthrich, E., Seward, D., Burg, J.P., Stockli, D., 2015. Low-temperature constraints on the Cenozoic thermal evolution of the southern Rhodope Core Complex (northern Greece). *Int. J. Earth Sci. (Geol. Rundsch.)* 104, 1337–1352.
- Koymans, M.R., Langereis, C.G., Pastor-Galán, D., Van Hinsbergen, D.J.J., 2016. Paleomagnetism.org: an online multi-platform open source environment for paleomagnetic data analysis. *Comput. Geosci.* 93, 127–137.
- Larrasoña, J.C., Roberts, A.P., Rohling, E.J., Winkhofer, M., Wehausen, R., 2003. Three million years of monsoon variability over the northern Sahara. *Clim. Dyn.* 21, 689–698.
- Laskar, J., Robutel, P., Joutel, F., Gastineau, M., Correia, A., Levrard, B., 2004. A long-term numerical solution for the insolation quantities of the earth. *Astron. Astrophys.* 428 (1), 261–285.
- Li, Y., Spassov, N., 2017. A new species of *Paramachaerodus* (Mammalia, Carnivora, Felidae) from the late Miocene of China and Bulgaria, and revision of *Promegantereon kretzoi*, 1938 and *Paramachaerodus pilgrim*, 1913. *Paläontol. Z.* 91 (3), 409–426.
- Liu, J., Li, J.J., Song, C.H., Yu, H., Peng, T.J., Hui, Z.C., Ye, X.Y., 2016. Palynological evidence for late Miocene stepwise aridification on the northeastern Tibetan plateau. *Clim. Past* 12, 1473–1484.
- López Martínez, N., 1989. Revisión sistemática y biostratigráfica de los Lagomorpha (Mammalia) del Terciario y Cuaternario de España. *Memorias del Museo Paleontológico de la Universidad de Zaragoza* 3, 1–342.
- López-Martínez, N., 1976. Lagomorpha from the Turolian of Pikerimi (Greece). In: *Proceedings of the Annual Meeting Chinese Society of Vertebrate Paleontology*. vol. B76. pp. 235–244.
- Mariolakis, I., Zagorchev, I., Fountoulis, I., Ivanov, M., 2004. Neotectonic transect Moesia-Apulia. Field trip guide book – B26. In: 32nd Int. Geol. Congr., Precongr. Field tRIP B26, (72 p).
- McFadden, P.L., McElhinny, M.W., 1988. The combined analysis of remagnetization circles and direct observations in paleomagnetism. *Earth Planet. Sci. Lett.* 87, 161–172.
- Mullender, T.A.T., Velzen, A.J., Dekkers, M.J., 1993. Continuous drift correction and separate identification of ferrimagnetic and paramagnetic contributions in thermomagnetic runs. *Geophys. J. Int.* 114, 663–672. <https://doi.org/10.1111/j.1365-246X.1993.tb06995.x>.
- Mullender, T.A.T., Frederichs, T., Hilgenfeldt, C., de Groot, L.V., Fabian, K., Dekkers, M.J., 2016. Automated paleomagnetic and rock magnetic data acquisition with an inline horizontal “2G” system. *Geochim. Geophys. Geosyst.* 17, 1–14. <https://doi.org/10.1002/2016GC006436>. Received.
- Nedialkov, P., Cheremisina, N., Kojumdjieva, E., Tzatzev, B., 1986. Facial and palaeogeographical characteristics of Neogene sediments in the Sandanski graben. *Geol. Balcanica* 16 (1), 69–80 (in Russian).
- Nesin, V.A., Nadachowski, A., 2001. Late Miocene and Pliocene small mammal faunas (Insectivora, Lagomorpha, Rodentia) of southeastern Europe. *Acta Zool. Cracovensia* 42, 107–135.
- Nikolov, I., 1985. Catalogue of the localities of tertiary mammals in Bulgaria. *Palaeontol. Stratigr. Lithol.* 21, 43–62 (in Bulgarian and English).
- Palcu, D.V., Vasilev, I., Stoica, M., Krijgsman, W., 2018. The end of the great drying of Eurasia: magnetostratigraphic dating of the Maeotian transgression in the eastern Paratethys. *Basin Res.* <https://doi.org/10.1111/bre.12307>. (in review).
- Pérouse, E., Wernicke, B.P., 2017. Spatiotemporal evolution of fault slip rates in deforming continents: the case of the Great Basin region, northern basin and range province. *Geosphere* 13 (1), 112–135.
- Pimpirev, C., Beratis, I., 2010. Lithostratigraphy of the Miocene sedimentary sequences in Strymon basin, northern Greece. *Comptes rendus de l'Académie bulgare des sciences. Geol. Stratigr.* 63 (8), 1177–1190.
- Popov, S.V., Nevesskaya, L.A., 2000. Late Miocene brackish water mollusks and the history of the Aegean basin. *Stratigr. Geol. Correl.* 8 (2), 195–205.
- Ravnäs, R., Steel, R.J., 1998. Architecture of marine Rift-Basin successions. *AAPG Bull.* 82 (1), 110–146.
- Roussiakis, S., 2009. *Prostrepsicerus* and *Protragelaphus* (Artiodactyla, Mammalia) from the late Miocene locality of Chomateri (Attica, Greece). *Ann. Paléontol.* 95, 181–195.
- Ruiz-Sánchez, F.J., Freudenthal, M., Mansino, S., Crespo, V.D., Montoya, P., 2014. *Apocricetus* *barrierei* (Rodentia, Mammalia) from La Bullana 2B and La Bullana 3 (Cabríel Basin, Valencia, Spain). Revision of the late Miocene–early Pliocene forms of the genus *Apocricetus*. *Paläontol. Z.* 88, 85–98.
- Sinitisa, M.V., 2010. Cricetids (Mammalia, Rodentia) from the upper Miocene of Egorovka locality. *Vestnik Zool.* 44 (3), 209–225 (in Russian).
- Sinitisa, M.V., 2012. Cricetids (Mammalia, Rodentia) from the upper Miocene locality of Palievo in the southern Ukraine. *Vestnik Zool.* 46 (2), 137–147 (in Russian).
- Snel, E., Măruțeanu, M., Meulenkamp, J.E., 2006. Calcareous nannofossil biostratigraphy and magnetostratigraphy of the upper Miocene and lower Pliocene of the northern Aegean (Orphanic gulf-Strimon Basin areas), Greece. *Palaeogeogr. Palaeoclimatol. Palaeoecol.* 238, 125–150.
- Spassov, N., 2002. The Turolian megafauna of West Bulgaria and the character of the late Miocene “Pikermian biome”. *Boll. Soc. Paleontol. Ital.* 41 (1), 69–81.
- Spassov, N., Geraads, D., Kovachev, D., 2004. *Tragoptax pilgrim* and *Miotragocerus* (*Pikermicerus*) *kretzoi* (Mammalia, Bovidae) from the Turolian of Bulgaria. *Geol. Balcanica Sofia* 34 (3–4), 89–109.
- Spassov, N., Tzankov, T., Geraads, D., 2006. Late Neogene stratigraphy, biochronology, faunal diversity and environments of south-West Bulgaria (Struma River valley). *Geodiversitas* 28 (3), 477–498.
- Spassov, N., Geraads, D., Hristova, L., Markov, G.N., Merceron, G., Tzankov, T., Stoyanov, K., Böhme, M., Dimitrova, A., 2012. A hominid tooth from Bulgaria: the last pre-human hominid of continental Europe. *J. Hum. Evol.* 62 (2), 138–145.
- Spassov, N., Böhme, M., Geraads, D., Kötter, S., van Baak, C., 2017. Pliocene mammal event, post-Pikermian mammal turnover and appearance of *Graecopithecus*. In: 5th Congress of the RCMNS. September 03-06.2017. Book of Abstracts, pp. 21.
- Spassov, N., Geraads, D., Hristova, L., Markov, G., Garevska, B., Garevski, R. (in press) **The late Miocene mammal faunas of the Republic of Macedonia (FYROM). Palaeontographica A.**
- St. John, K.E.K., Krisek, L.A., 2002. The late Miocene to Pleistocene ice-rafting history of Southeast Greenland. *Boreas* 31, 28–35.
- Stübner, K., Drost, K., Schoenberg, R., Böhme, M., Starke, J., Ehlers, T.A., 2016. Asynchronous timing of extension and basin formation in the south Rhodope core complex. *SW Bulgaria Northern Greece Tectonics* 35, 136–159. <https://doi.org/10.1002/2015TC004044>.
- Stuut, J.-B., Smalley, I., O'Hara-Dhand, K., 2009. Aeolian dust in Europe: African sources and European deposits. *Quat. Int.* 198, 234–245.
- Theodorou, G.E., Roussiakis, S.J., Athanassiou, A., Filippidi, A., 2010. Mammalian remains from a new site near the classical locality of Pikerimi (Attica, Greece). In: *Scientific Annals, School of Geology, Aristotle University of Thessaloniki, Proceedings of the XIX CBGA Congress, Thessaloniki, Greece*. vol. 99. pp. 109–119.
- Thomas, H., Spassov, N., Kojumdjieva, E., Poidevin, J.-L., Sen, S., Tassy, P., Visset, D., 1986. Résultats préliminaires de la première mission paléontologique franco-bulgare à Dorkovo (arrondissement de Pazardjik, Bulgarie). *Comptes Rendus de l'Académie des Sciences Paris Série II* 302, 1037–1042.
- Topachevski, V.A., Skorik, A.F., 1992. Neogene and Pleistocene Primitive Cricetoids of Southern Eastern Europe. *Naukova Dumka Press, Kiev* 242 p. (in Russian).
- Tzankov, T., Spassov, N., Stoyanov, K., 2005. Neogene-Quaternary Paleogeography and Geodynamics of Middle Struma River Valley Area (S.-W. Bulgaria). *South-West University “N. Rilski”, Blagoevgrad* (199 p, in Bulgarian with English summary).
- Tzanova, A., Herbert, T.D., Peterson, L., 2015. Cooling Mediterranean Sea surface temperatures during the late Miocene provide a climate context for evolutionary transitions in Africa and Eurasia. *Earth Planet. Sci. Lett.* 419, 71–80.
- Van Dam, J.A., Alcalá, L., Alonso Zarza, A., Calvo, J.P., Garcés, M., Krijgsman, W., 2001. The upper Miocene mammal record from the Teruel-Alfambra region (Spain). The MN system and continental stage/age concepts discussed. *J. Vertebrate Paleontol.* 21 (2), 367–385.
- Vandenberghe, J., 2013. Grain size of fine-grained windblown sediment: a powerful proxy for process identification. *Earth-Sci. Rev.* 121, 18–30.
- Vangengeim, E.A., Tesakov, A.S., 2008. Maeotian mammalian localities of eastern Paratethys: Magnetostratigraphy and position in European continental scales. *Stratigr. Geol. Correl.* 16 (4), 437–450.
- Vasileiadou, K., Koufos, G.D., Syrides, G.E., 2003. Silata, a new locality with micro-mammals from the Miocene/Pliocene boundary of the Chalkidiki peninsula, Macedonia, Greece. *DEINSEA* 10, 549–562.
- Vasileiadou, K., Konidaris, G., Koufos, G.D., 2012. New data on the micromammalian locality of Kessani (Thrace, Greece) at the Mio-Pliocene boundary. *Palaeobiodiversity Palaeoenvironments* 92, 211–237.
- Vrablianski, B., 1969. The Melnik fault and its neotectonic importance. *Izvestia Geol. Inst. Bulgarian Acad. Sci.* 18, 167–172 (in Bulgarian).
- Weltje, G.J., Prins, M.A., 2007. Genetically meaningful decompositions of grain-size distributions. *Sed. Geol.* 231 (3), 409–424.
- Westaway, R., 2006. Late Cenozoic extension in SW Bulgaria: a synthesis. *Geol. Soc. Lond. Spec. Publ.* 260 (1), 557–590.
- Zagorchev, I., 1992. Neotectonic development of the Struma (Kraigtid) lineament, southwest Bulgaria and northern Greece. *Geol. Mag.* 129, 197–222.
- Zagorchev, I., 2001. Geology of SW Bulgaria: an overview. *Geol. Balcanica* 21 (1–2), 3–52.
- Zagorchev, I., 2007. Late Cenozoic development of the Struma and Mesta fluvio-lacustrine systems, SW Bulgaria and northern Greece. *Quat. Sci. Rev.* 26 (22), 2783–2800.
- Zagorchev, I., Dinkova, J., 1990. Geological map of the People's Republic of Bulgaria, 1:100,000 series Petrich, Razlog, Blagoevgrad, Gotse Delchev and Belitsa sheets. Geological Institute, Bulgarian Academy of Sciences, Sofia.